

Excitation with quantum light. II. Exciting a two-level system

J. C. López Carreño,¹ C. Sánchez Muñoz,¹ E. del Valle,¹ and F. P. Laussy^{2,1}

¹*Departamento de Física Teórica de la Materia Condensada, Universidad Autónoma de Madrid, 28049 Madrid, Spain*

²*Russian Quantum Center, Novaya 100, 143025 Skolkovo, Moscow Region, Russia*

(Received 3 September 2016; published 13 December 2016)

We study the excitation of a two-level system (2LS) by quantum light, thereby bringing our previous studies [see Paper I of this series, *Phys. Rev. A* **94**, 063825 (2016)] to a target that is quantum itself. While there is no gain for the quantum state of the target as compared to driving it with classical light, its dynamical features, such as antibunching, can be improved. We propose a chain of two-level systems, i.e., setting the emission of each 2LS as the driving source of the following one, as an arrangement to provide better single-photon sources. At a fundamental level, we discuss the notion of strong coupling between quantum light from a source and its target, and the several versions of the Mollow triplet that follow from various types of driving light. We discuss the Heitler effect of antibunched photons from the scattered light off a laser.

DOI: [10.1103/PhysRevA.94.063826](https://doi.org/10.1103/PhysRevA.94.063826)

I. INTRODUCTION

The two-level system (also known as the “two-state quantum system” [1]) is an important type of oscillator in the quantum universe. In some respects, it can be seen as the truly quantum oscillator, with a response at the single-particle level, whereas the (quantum) harmonic oscillator appears instead as a classical oscillator able to sustain nonclassical motion. The two-level system (2LS), a fundamental object in any case, rose to gigantic proportion with Deutsch’s insight of quantum computation [2], that turned it into a “qubit,” the elementary piece of information in the physical universe. It then became of primary importance to control the dynamics of a two-level system. To this day, this is achieved mainly with classical laser pulses, thanks to a “pulse-area” theorem that states that any desired final state can be obtained with a suitable pulse [3]. Entire textbooks have been written on the topic [4] and still have not exhausted it.

In this text, second in a series where we address the general problem of exciting with quantum light [5], we study the excitation of the 2LS (or qubit) when driven quantum mechanically, rather than classically. We focus in the present text on cw excitation and refer to future work for pulsed excitation, of particular relevance for state preparation and quantum information processing. We will show that while the quantum states that can be prepared in a 2LS with the source of quantum excitation are not different than those accessible with the classical excitation, the dynamical emission on the other hand can reach new regimes. As an application, we will show how this can be used to engineer better single-photon sources. To a large extent, the problem posed in this text also addresses the fundamental question of what defines strong coupling. The excitation of a 2LS by light falls largely in the framework of resonance fluorescence, whose most notable manifestation is the so-called Mollow triplet [6]. This occurs when the intense excitation (by a classical laser) of a 2LS dresses its bare states (ground $|g\rangle$ and excited $|e\rangle$) to give rise to new eigenstates from their quantum superposition $|\pm\rangle \equiv (|g\rangle \pm |e\rangle)/2$. The coupling is mediated by the classical laser that, being a c -number parameter, does not directly appear in the structure of the Hilbert space and thus neither in the quantum state. We will discuss in detail the nature of these dressed states when quantizing the excitation field and how various quantum states leads to various results.

The text is organized as follows. Section II briefly reminds the formalism which has been amply motivated and introduced in Paper I (Secs. I and II) [5] and we refer to this text and references therein for further details. In Sec. III, we study which states of the 2LS are accessible under quantum excitation where we show how, in the cw regime, classical excitation is more suitable than driving by, say, a single-photon source (SPS), in terms of the accessible states in the Bloch sphere. In Sec. IV, we discuss how strong coupling takes place with the more general case of quantum light as the driving agent. Beyond a new definition for strong coupling needed to accommodate quantization of the driving light field, this discussion will also allow us to pinpoint which features are specific to the classical driving by contrasting all the variants of the Mollow triplet under various types of excitation. For instance, we will shed light on the mysterious Heitler effect whereby coherent absorption-emission processes in the low driving limit result in photons with the first-order coherence of the source (the laser) and the second-order coherence of the target (the 2LS). Since such a source of spectrally narrow antibunched photons is of high technological interest, the understanding of its underlying principle is important. In Sec. V, we take advantage of this understanding to design better SPS by turning the target into a source of its own, that excites still another 2LS. We will show how better antibunching can be achieved in this way that overcomes the Rayleigh scattering. Section VI concludes.

II. THEORETICAL DESCRIPTION

Like in Paper I [5], we use the cascaded formalism to describe the irreversible excitation of a target by a quantum source. Here, we focus on a 2LS as the target (with annihilation operator ξ) and consider various sources that will be introduced as they are referred to. Taking for instance another 2LS with annihilation operator σ as the source, as sketched in Fig. 1(a), the resulting master equation takes the form (we take $\hbar = 1$ along the paper):

$$\begin{aligned} \partial_t \rho = & i[\rho, H_\sigma + H_\xi] + \frac{\gamma_\sigma}{2} \mathcal{L}_\sigma \rho + \frac{\gamma_\xi}{2} \mathcal{L}_\xi \rho \\ & + \sqrt{\gamma_\sigma \gamma_\xi} \{[\sigma \rho, \xi^\dagger] + [\xi, \rho \sigma^\dagger]\}. \end{aligned} \quad (1)$$

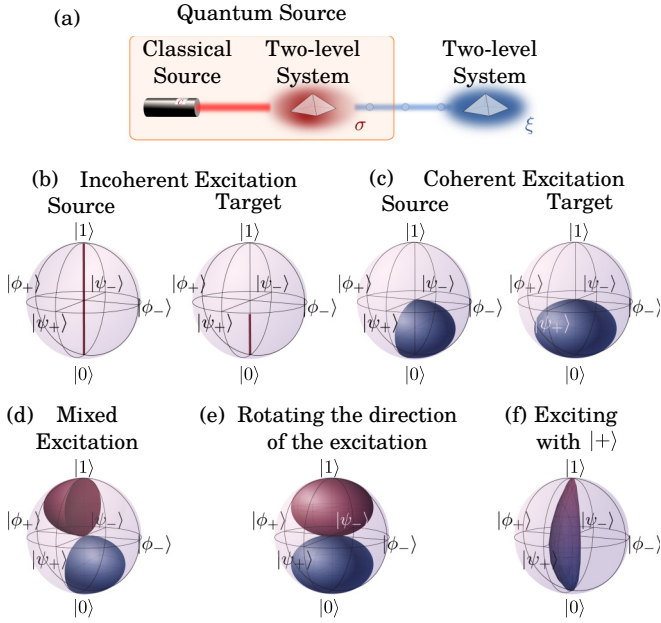


FIG. 1. (a) A 2LS is driven by the emission of a quantum source. In this particular case, the quantum source is made of a 2LS driven by a classical source. (b)–(f) Accessible states of the 2LS under different driving configurations, as seen by the accessible volume in the Bloch sphere. The states of the equator of the sphere are $|\psi_{\pm}\rangle = (|0\rangle \pm |1\rangle)/\sqrt{2}$ and $|\phi_{\pm}\rangle = (|0\rangle \pm i|1\rangle)/\sqrt{2}$. (b) Incoherent excitation: this kind of excitation does not generate coherence in the 2LS, so all the accessible states lie along the z axis of the Bloch sphere. (c) Coherent excitation: this kind of excitation does not allow the qubit to have a population larger than $\frac{1}{2}$, so all the accessible states lie in the south hemisphere of the Bloch sphere. The source 2LS is allowed to go only in one half of the ellipsoid, while the target 2LS can cover the ellipsoid completely. (d) Mixed excitation: under this driving the source 2LS can access a symmetrical region in the north hemisphere of the Bloch sphere. However, the region available to the target 2LS does not increase. (e) Rotating the direction of the excitation of the source 2LS allows it to access the regions otherwise out of reach, thus filling the entire ellipsoid. (f) Exciting with $|+\rangle\langle 0|$ allows the source 2LS to access states with mean population $\frac{1}{2}$ but not completely mixed.

Here, $\mathcal{L}_c\rho = (2c\rho c^\dagger - \rho c^\dagger c - c^\dagger c\rho)$, where $c = \sigma$ for the source and $c = \xi$ for the target, with σ, ξ following the Pauli algebra. Each system has a decay rate and a Hamiltonian, labeled γ_c and H_c . The source must also be excited, and the details and considerations required to describe properly the driving of the source are presented in Sec. II of Paper I [5]. We now proceed to investigate which regions of the Bloch sphere are accessible under various types of driving.

III. ACCESSIBLE STATES

While we had to introduce in Paper I of the series a new charting of the harmonic oscillator's Hilbert space to map the states created by quantum excitation, there has long been a comprehensive representation for the two-dimensional Hilbert space of the qubit: the *Bloch sphere*, that allows to map unambiguously pure states since the sphere is the projective

space for two complex lines [7] $(\alpha, \beta) \in \mathbb{C}^2$ and pure states of the 2LS are given by the wave function:

$$|\psi\rangle = \alpha|0\rangle + \beta|1\rangle. \quad (2)$$

The mapping is complete since it also accounts for the phase between the probability amplitudes. The quantum dynamics of a 2LS also evolves naturally in this geometry [8], also accommodating mixed states *inside* the Bloch sphere (pure states lie on its surface). Mixed states are expressed by a density matrix, which is also determined by two numbers, the population and the coherence of the qubit:

$$\rho = \begin{pmatrix} 1 - n_\sigma & \langle\sigma\rangle^* \\ \langle\sigma\rangle & n_\sigma \end{pmatrix}, \quad (3)$$

where $n_\sigma \equiv \langle\sigma^\dagger\sigma\rangle$, the 2LS population, is such that $0 \leq n_\sigma \leq 1$, and $\langle\sigma\rangle$, the coherence of the qubit, is a complex number. Since the eigenvalues of the density matrix must be non-negative, the coherence of the qubit has an upper bound: $|\langle\sigma\rangle|^2 \leq n_\sigma(1 - n_\sigma)$. The state in Eq. (3) is pure if $\text{Tr}(\rho^2) = 1$, i.e., if $|\langle\sigma\rangle|^2 = n_\sigma(1 - n_\sigma)$, in which case the states in Eqs. (2) and (3) are equivalent, with $n_\sigma = |\beta|^2$ and $\langle\sigma\rangle = \alpha\beta^*$. Thus, any state in the form of Eq. (3) is represented in the Bloch sphere as a point with Cartesian coordinates:

$$x = 2\mathcal{R}\langle\sigma\rangle, \quad y = -2\mathcal{I}\langle\sigma\rangle, \quad \text{and} \quad z = 1 - 2n_\sigma, \quad (4)$$

such that $x^2 + y^2 + z^2 \leq 1$. The amount of vacuum and excitation, often referred to as *population imbalance*, varies along the z axis. The relative phase between the vacuum and the excited state is given by $\phi = \arg\langle\sigma\rangle$ and varies around the x - y plane.

A. Incoherent driving

To contrast the excitation of a 2LS by quantum light with the usual counterpart of classical excitation, we must first remind (and in some cases possibly derive) the situation in the latter case. We will see throughout that the need to understand the quantum excitation also teaches us features of the more familiar classical case.

The expected value of the coherence $\langle\sigma\rangle$ of an incoherently driven 2LS is zero, so its steady-state density matrix is fully determined only by its population:

$$n_\sigma^{\text{inc}} = \frac{P_\sigma}{P_\sigma + \gamma_\sigma}, \quad (5)$$

where P_σ is the rate of incoherent driving. The accessible states under incoherent excitation cover the entire z axis, as shown in the Bloch sphere on the left in Fig. 1(b). Using this 2LS as a source for another 2LS reduces the span of accessible area. Namely, the steady state of the target 2LS, also determined only by its population, reads:

$$n_\xi^{\text{inc}} = \frac{4n_\sigma^{\text{inc}}\gamma_\sigma(P_\sigma + \gamma_\sigma + \gamma_\xi)}{P_\sigma^2 + (\gamma_\sigma + \gamma_\xi)^2 + 4\Delta_{\sigma\xi}^2 + 2P_\sigma(\gamma_\xi + 5\gamma_\sigma)}, \quad (6)$$

where γ_ξ is the decay rate of the target 2LS, and $\Delta_{\sigma\xi} = \omega_\sigma - \omega_\xi$ is the detuning between the source and the target. The accessible states are shown in the Bloch sphere on the right in Fig. 1(b), and unlike the source 2LS that can be saturated to its excited state by incoherent pumping, the population of the target 2LS lies between $0 \leq n_\xi^{\text{inc}} \leq 0.3535$.

The upper bound 0.3535 is obtained in the regime $P_\sigma \approx \gamma_\sigma$ for the source, in which case $n_\sigma^{\text{inc}} = \frac{1}{2}$, and when $\gamma_\xi \approx \gamma_\sigma$. The reason for this saturation is a type of self-quenching, here induced by the power broadening of the source. This shows clearly the intrinsic limitations of exciting with a 2LS. One can increase the emission rate, but this comes at the expense of other fundamental parameters such as the spectral broadening. In contrast, one can increase the emission rate of a cavity independently of its spectral width.

B. Coherent driving

In the case of coherent classical driving of the source, its population and coherence are given by:

$$n_\sigma^{\text{coh}} = \frac{4\epsilon_1 \Omega^2}{\gamma_\sigma^2 + 4\tilde{\omega}_\sigma^2 + 8\epsilon_1 \Omega^2}, \quad (7a)$$

$$\langle \sigma \rangle^{\text{coh}} = \frac{2\sqrt{\epsilon_1} \Omega (2\tilde{\omega}_\sigma + i\gamma_\sigma)}{\gamma_\sigma^2 + 4\tilde{\omega}_\sigma^2 + 8\epsilon_1 \Omega^2}, \quad (7b)$$

where Ω is the rate of coherent excitation, ϵ_1 is the amplitude of the channel through which we drive coherently the source, and $\tilde{\omega}_\sigma$ is the detuning between the driving laser and the

2LS. Unlike the incoherent excitation, these states now span a volume in the Bloch sphere, which means that they have some degree of purity, the higher the closer to the ground state. Also, since coherent driving forbids population inversion, this volume is restricted to the south hemisphere of the Bloch sphere, reaching population $n_\sigma = \frac{1}{2}$ at most in a maximally mixed state. Finally, the phase of the driving laser also fixes the phase of the excitation of the 2LS, so only one half of the southern hemisphere is accessible. The final accessible volume is shown in the left Bloch sphere in Fig. 1(c). Its boundaries are given by the shell of an ellipsoid with equation:

$$1 = \left(\frac{x}{\sqrt{2}/2} \right)^2 + \left(\frac{y}{\sqrt{2}/2} \right)^2 + \left(\frac{z - z_0}{1/2} \right)^2, \quad (8)$$

with $z_0 = -\frac{1}{2}$, $|x| \leq \sqrt{2}/2$, and $-\sqrt{2}/2 \leq y \leq 0$.

The expressions for the population and coherence of the target 2LS are not as straightforward as for the source 2LS, and although they can be found in closed form, they are too lengthy to be written here. As an illustration of their complexity, we provide the particular case when the driving laser, the source 2LS, and the target 2LS are in resonance, in which case the population and the coherence of the target 2LS reduce to:

$$n_\xi^{\text{coh}} = 16\epsilon_1 \Omega^2 (1 - \epsilon_1) \gamma_{\tilde{0}} \{ \gamma_{\tilde{1}}^3 \gamma_{\tilde{2}} \gamma_{\tilde{2}} + 8\epsilon_1 \Omega^2 [2\gamma_{\tilde{0}}^3 + 6\gamma_{\tilde{0}}^2 \gamma_{\tilde{0}} + \gamma_{\tilde{0}} \gamma_{\tilde{0}}^2 (1 - \epsilon_1) + 3\gamma_{\tilde{0}}^3] + 64\gamma_{\tilde{0}} \epsilon_1^2 \Omega^4 \} / N^*, \quad (9a)$$

$$\langle \xi \rangle^{\text{coh}} = -4i \sqrt{\gamma_{\tilde{0}} \gamma_{\tilde{0}} \epsilon_1 (1 - \epsilon_1) \Omega} \gamma_{\tilde{0}} \{ \gamma_{\tilde{1}}^3 \gamma_{\tilde{2}} \gamma_{\tilde{2}} + 8\gamma_{\tilde{1}}^2 \epsilon_1 \Omega^2 [4\gamma_{\tilde{0}} + \gamma_{\tilde{0}} (8\epsilon_1 - 3)] + 128\epsilon_1^2 \Omega^4 [\gamma_{\tilde{0}} + \gamma_{\tilde{0}} (2\epsilon_1 - 1)] \} / N^*, \quad (9b)$$

with

$$N^* = \gamma_{\tilde{0}} \gamma_{\tilde{0}}^2 \gamma_{\tilde{1}}^3 \gamma_{\tilde{2}} \gamma_{\tilde{2}} + 8\gamma_{\tilde{1}}^2 \epsilon_1 \Omega^2 [2\gamma_{\tilde{0}}^4 + 7\gamma_{\tilde{0}}^3 \gamma_{\tilde{0}} + 12\gamma_{\tilde{0}}^2 \gamma_{\tilde{0}}^2 + 2\gamma_{\tilde{0}} \gamma_{\tilde{0}}^3 (13 - 10\epsilon_1) + 8\gamma_{\tilde{0}}^4 (1 - \epsilon_1)] + 64\epsilon_1^2 \Omega^4 [5\gamma_{\tilde{0}}^4 + 2\gamma_{\tilde{0}} \gamma_{\tilde{0}}^3 (23 - 20\epsilon_1) + 3\gamma_{\tilde{0}}^2 \gamma_{\tilde{0}}^2 (21 - 16\epsilon_1) + 2\gamma_{\tilde{0}}^3 \gamma_{\tilde{0}} (17 - 10\epsilon_1) + 8\gamma_{\tilde{0}}^4] + 1024\epsilon_1^3 \Omega^6 [\gamma_{\tilde{0}}^2 + \gamma_{\tilde{0}} \gamma_{\tilde{0}} (3 - 2\epsilon_1)], \quad (9c)$$

where we have introduced the notation:

$$\gamma_{mn}^k \equiv (m\gamma_\sigma + n\gamma_\xi)^k, \quad (10)$$

e.g., $\gamma_{\tilde{2}}^2 = (2\gamma_\sigma + \gamma_\xi)^2$. Interestingly, while Eqs. (9) for the target have a much more complicated form than Eqs. (7) for the source, they lead to the same accessible volume of the type of Eq. (8). As such, unlike the case of incoherent excitation, the target suffers no restriction of its accessible region under quantum excitation by a coherently excited 2LS as compared to direct excitation from the coherent source. In fact, since the phase of excitation is not fixed by the source, the accessible volume of the target 2LS is given by the full ellipsoid in Eq. (8) with $|y| \leq \sqrt{2}/2$, as shown in the right Bloch sphere of Fig. 1(c).

C. Mixture of coherent and incoherent driving

The source 2LS can drive its target from the entire z axis when driven incoherently to half an ellipsoid in the southern hemisphere when driven coherently. Mixing the two types of excitations allows the source 2LS to access a volume in the northern hemisphere as well, symmetric to the volume accessible by coherent excitation only, as shown in Fig. 1(d).

The expressions for the population and the coherence in this case are:

$$n_\sigma^{\text{mix}} = \frac{P_\sigma [(P_\sigma + \gamma_\sigma)^2 + 4\tilde{\omega}_\sigma^2] + 4\epsilon_1 \Omega^2 (P_\sigma + \gamma_\sigma)}{(P_\sigma + \gamma_\sigma) [(P_\sigma + \gamma_\sigma)^2 + 4\tilde{\omega}_\sigma^2 + 8\epsilon_1 \Omega^2]}, \quad (11a)$$

$$\langle \sigma \rangle^{\text{mix}} = \frac{2\sqrt{\epsilon_1} \Omega (P_\sigma - \gamma_\sigma) [2\tilde{\omega}_\sigma + i(P_\sigma + \gamma_\sigma)]}{(P_\sigma + \gamma_\sigma) [(P_\sigma + \gamma_\sigma)^2 + 4\tilde{\omega}_\sigma^2 + 8\epsilon_1 \Omega^2]}, \quad (11b)$$

from which we see that the condition to access the volume in the northern hemisphere, i.e., $n_\sigma \geq \frac{1}{2}$, is simply that $P_\sigma > \gamma_\sigma$. The northern-hemisphere volume is enclosed by the ellipsoid in Eq. (8) with $z_0 = \frac{1}{2}$, $|x| \leq \sqrt{2}/2$, and $0 \leq y \leq \sqrt{2}/2$.

Using this 2LS under joint coherent and incoherent driving to bring its steady state off axis in the northern hemisphere does not, however, make it a quantum source that can drive a target 2LS beyond the southern-hemisphere ellipsoid of coherent excitation [Fig. 1(c)]. The expressions for the population and coherence of the target 2LS in this case are analytical as well, but even at resonance and using the compact notation of Eq. (10), they are too bulky to be written here. Note that by changing the direction from which the laser drives the source 2LS, or by using wave plates, one can rotate its phase, changing σ for $e^{i\theta}\sigma$ in the master equation (1). This variation leaves the population of the source 2LS unchanged, but adds

a phase to its coherence. In this way, the source 2LS can span all states in a volume obtained by revolving around the z axis. The same holds for the case of mixed excitation, and therefore the total accessible volume of the source 2LS is given by two full ellipsoids as shown in Fig. 1(e).

Overall, these results show that a 2LS as a source of excitation is no more advantageous than classical sources as far as accessible volumes in the Bloch sphere and in the steady state are concerned. The target is “quantum enough” not to benefit further from quantum excitation (at least when it comes from a SPS) as compared to classical excitation. We will see later in the text that this is because we consider the target in isolation, and that including quantum correlations with the source indeed leads to departures and benefits from a quantum driving. In the next paragraph, we also anticipate on more general results to be presented in future work of this Series that considers the excitation from more exotic quantum sources than simply a SPS, in which case, the target’s quantum state can depart from the classical driving cases.

D. Phenomenological quantum source

So far, we have modeled the quantum source by describing it fully and self-consistently, coupling its output to a target through the cascaded formalism. The excitation of the source itself was achieved phenomenologically from the Lindblad formalism. One could also in principle take a simpler route by describing directly the quantum source through *ad hoc* Lindblad terms. This is an expedient way to see whether quantum excitation can bring us to regions beyond those of access from the classical case, that lie in an ellipsoid of, for most of the cases, mixed states (not on the surface of the sphere). In particular, a common feature of all the kinds of excitation we have considered is that the state with population $\frac{1}{2}$ is completely mixed, i.e., it is located at the origin of the sphere.

We now show how to drive the target 2LS to reach states with population $\frac{1}{2}$ but with nonzero coherence. Specifically, we assume a source that emits photons in the state $|+\rangle_\phi = (|0\rangle + e^{i\phi}|1\rangle)/\sqrt{2}$. At the simplest level, the incoherent type of such an excitation is described with Lindblad terms in the master equation (1) of the type $(P^*/2)\mathcal{L}_x\rho$, where $x = |+\rangle_\phi\langle 0|$ is the operator that brings the vacuum state into $|+\rangle_\phi$, and P^* is the rate at which this excitation is enforced onto the target. The resulting population and coherence of the source 2LS in this case are given by:

$$n_\sigma^+ = \frac{P^*(P^* + 2\gamma_\sigma e^{i\phi})}{P^{*2} + 4\gamma_\sigma^2 + 4P^*\gamma_\sigma \cos 2\phi}, \quad (12a)$$

$$\langle\sigma\rangle^+ = \frac{2P^*\gamma_\sigma}{(P^* + \gamma_\sigma)(P^*e^{2i\phi} + 2\gamma_\sigma)}, \quad (12b)$$

where the phase ϕ must be chosen so that $n_\sigma^+ \in \mathbb{R}$. The accessible volume with $\phi = 0$ is shown in Fig. 1(f). This case demonstrates a type of quantum excitation that drives the 2LS target into a volume of the Bloch sphere that strongly differs from the classical counterpart. The cw excitation spoils the coherence, and even a source that explicitly drives the 2LS into the $|+\rangle$ state cannot sustain completely its coherence of the 2LS. Nevertheless, this indicates that the general case of

quantum excitation does ultimately bring us further than the classical case, even though the SPS does not. Importantly, to clarify this point at this stage, we have assumed a simple phenomenological model for a particular case. It is not clear how such a source could be devised from a Hamiltonian in the first place before it is plugged to its target through the cascaded formalism. For instance, a close counterpart that emits photons in the state $|+\rangle_\phi = (|0\rangle + e^{i\phi}|1\rangle)/\sqrt{2}$ with a complex superposition ($\phi \notin \{0, \pi\}$), that is easily conceived conceptually, cannot be described in the above Lindblad form since this results in nonreal coefficients of the master equation that yield unphysical density matrix (and, e.g., complex populations).

IV. MOLLOW DRESSING

A. Introduction

In this section, we go beyond which average quantum state a target 2LS can be driven into to consider instead some deeper structural aspect, namely, we describe the energy spectrum and its associated set of states. The naked 2LS has the simplest possible structure of a vacuum $|g\rangle$ and an excited state $|e\rangle$. When placed inside a cavity, in absence of dissipation, a new set of quantum states for the combined system takes over, that are eigenvectors for the coupling Hamiltonian [9]: $(|g, n\rangle + |e, n-1\rangle)/\sqrt{2}$ at resonance with n the number of photons in the cavity. The respective pair of energies constitutes one stair of the so-called Jaynes-Cummings ladder, that repeats this structure for each integer n . These states are entangled and go by the name of “polaritons” or “dressed states.” In presence of dissipation, a notion of weak and strong coupling emerges to distinguish cases where bare states $|g, e\rangle$ and $|n\rangle$ dominate the dynamics as dissipation destroyed their quantum superpositions. In the former case, the coupling is classical while in the latter it binds the states through quantum superposition. This is a central concept of cavity QED but one that remains vaguely defined as rooted in the simple Hamiltonian framework. When including dissipation, the dressed-states energies become complex as a result of their finite lifetime, and acquire a broadening specific to their constitution in terms of bare states in addition to a renormalized energy. This is well understood for two coupled oscillators but already the textbook case of the 2LS in a cavity displays a much less familiar structure, the so-called “dissipative Jaynes-Cummings ladder” [10], with coexistence of weak and strong coupling depending on the manifold of excitation. Such a description can be applied to other systems [11]. When including, beyond mere decay, also an excitation scheme, the situation can become extremely complex [12]. The simplest problem of this type is the celebrated Mollow triplet [6], where a 2LS is strongly excited by a classical field (c number). This is the context in which the term of “dressed state” appeared (from Cohen-Tannoudji [13]). In this text where we study quantum driving of a 2LS, we are naturally brought to consider how the quantum features of light affect the 2LS target’s state. In the limit where light is coherent, we expect to recover the conventional Mollow scenario, as is already known to be the case from the Jaynes-Cummings perspective where light is quantized [14].

We will now turn to the more general problem of how a 2LS target becomes affected by quantum excitation without

TABLE I. Classification of the shape of the emission of the target 2LS according to the source driving it.

Type of source	Shape of the 2LS target	Treated in
Classical laser	Mollow triplet	Sec. IV C
Two-level system excited incoherently	Unresolved Mollow triplet	Sec. IV D
Two-level system excited coherently	Mollow triplet with attenuated sidebands	Sec. IV E
Cavity spontaneous emission	Variant of the Mollow triplet	Op. V
Cavity excited incoherently	Deformed singlet	Sec. IV F
Cavity excited coherently	Mollow triplet	Sec. IV G
One-atom laser	Quintuplet to Mollow triplet transition	Sec. IV H
N -photon source	Quantum Mollow triplet	Op. IV

feedback, i.e., beyond the Hamiltonian formalism (the cases that will be dealt with are summarized in Table I). This poses some immediate questions such as the following: Can a single-photon source dress a 2LS? Are Rabi oscillations, exchanges of excitation between the modes, necessary for state dressing? If so, how can this be achieved in the cascaded formalism where feedback is precisely forbidden? Does the Mollow theory of a c -number description of the exciting laser break down in some regime, say of low excitation? These and other fundamental questions are answered in the remainder of this section.

B. Complex energy spectrum

We define strong coupling as the emergence of resonances in the system with real energies different from those of the bare states. Such resonances are obtained in a dissipative system from the eigenvalues D_p of the Liouvillian matrix M [15], that follows from writing Eq. (1) as:

$$\partial_t \{\rho\} = -M \{\rho\}, \quad (13)$$

where $\{\rho\}$ is the density matrix laid out in vectorial form, namely, $\{\rho\} = (\rho_{11}, \rho_{21}, \dots, \rho_{n1}, \rho_{21} \dots \rho_{nn})^T$ for some truncation n that can be taken to go to ∞ . This gives access to the “transitions” in the system, rather than directly to the energies of the states. This is a nuance already present in the first historical considerations of light-matter interactions [16]. From the knowledge of the transitions, however, one can usually reconstruct the underlying energy structure of the system, that is, both the composition of the dressed states and their associated energies. A typical observable is the total emission spectrum that results from the combined emission between the various states:

$$S(\omega) = \frac{1}{\pi} \sum_p \frac{(\gamma_p/2)L_p - (\omega_p - \omega)K_p}{(\gamma_p/2)^2 + (\omega_p - \omega)^2}, \quad (14)$$

where $\gamma_p/2 + i\omega_p \equiv D_p$ is the p th resonance, i.e., eigenvalue of M , that defines the energy structure of the system, and L_p and K_p are the corresponding weights for this transition that determine its prominence in the total emission accordingly with the state and dynamics of the system. The term L_p weights a pure Lorentzian emission, corresponding to spontaneous emission from the initial state towards the final one, while K_p brings a dispersive correction that is typical of coupled oscillators and that results in our case from interferences between transitions that overlap in energy. In finite-size Hamiltonian systems or those that can be decomposed into a direct sum of uncoupled manifolds, such as the Jaynes-Cummings Hamiltonian, the most important structure comes

from D_p alone. In infinite-size systems where the system cannot be closed in a self-consistent way, for instance, because an excitation term connects all the manifolds, one then needs to weight the transition D_p with $|L_p + iK_p|$ as otherwise different truncation schemes of M give different results for the complex energy spectrum, whereas the weighted transitions converge to a physical result. For this reason, the complex weight is fundamental as well. It is obtained as [15]:

$$L_p + iK_p = \frac{1}{n_\sigma} \text{Tr} \left\{ \sigma \left(E_{*p} \sum_n E_{pn}^{-1} \rho_{ss} \sigma^\dagger \right) \right\}, \quad (15)$$

where ρ_{ss} is the steady-state solution of the master equation, σ is the annihilation operator of the 2LS, $n_\sigma = \text{Tr}(\sigma^\dagger \sigma \rho_{ss})$ is its population, and E is the matrix of eigenvectors of M (i.e., $E^{-1}ME$ is the diagonal matrix of complex energies). Here, E_{*p} refers to the p -th column of matrix E , M_n refers to the n th element of the flattened matrix \mathcal{M} and (\mathcal{V}) refers to the reversed process that shapes the vector \mathcal{V} (of size n^2) into a matrix as $(\mathcal{V}_1, \mathcal{V}_2, \dots, \mathcal{V}_n), (\mathcal{V}_{n+1}, \mathcal{V}_{n+2}, \dots, \mathcal{V}_{2n}), \dots$.

In the following sections, we start a comprehensive analysis of the complex energy spectrum, and the structure of states (bare and dressed) associated to it, for the configurations of excitation of a 2LS listed in Table I. Namely, in Sec. [IV C](#) we start with the conventional Mollow triplet, where a classical field drives a 2LS, then in Sec. [IV D](#) we replace the classical field by the simplest quantum light, i.e., that emitted by a SPS; in Sec. [IV E](#), the SPS is brought itself in the Mollow triplet regime. Then, we come back to the conventional Mollow configuration of light exciting a 2LS, but with light described by an operator rather than by a c number. This will allow us to (i) see what is lost in the approximation of describing the laser as a sine wave and (ii) consider classical excitation beyond merely a coherent state. Specifically, we consider in Sec. [IV F](#) a thermal state of the light field (chaotic light), in Sec. [IV G](#) a coherent state (the closest to the conventional Mollow case), and, finally, in Sec. [IV H](#), we take an additional step in describing the quantum dynamics of an actual laser acting as the source to drive the 2LS, taking the simplest case of a one-atom laser to do so. All these cases bring some variations to the problem. Their common features give a picture of what constitutes the substance of the Mollow triplet.

C. Excitation by a classical field

The simplest classical excitation of a 2LS is that provided by a thermal source, or incoherent pumping, that brings the

system into its excited state at a rate P_σ . For completeness, we address this case as well before we turn to coherent excitation that leads to Mollow physics. The 2LS incoherently pumped is described by the master equation:

$$\partial_t \rho = i[\rho, \omega_\sigma \sigma^\dagger \sigma] + \frac{\gamma_\sigma}{2} \mathcal{L}_\sigma \rho + \frac{P_\sigma}{2} \mathcal{L}_{\sigma^\dagger} \rho, \quad (16)$$

where ω_σ is the free energy of the 2LS and γ_σ its decay rate (inverse lifetime of the excited state), with M matrix [in Eq. (13)]:

$$M = \begin{pmatrix} P_\sigma & 0 & 0 & -\gamma_\sigma \\ 0 & \Gamma_\sigma/2 + i\omega_\sigma & 0 & 0 \\ 0 & 0 & \Gamma_\sigma/2 + i\omega_\sigma & 0 \\ -P_\sigma & 0 & 0 & \gamma_\sigma \end{pmatrix}, \quad (17)$$

where $\Gamma_\sigma \equiv \gamma_\sigma + P_\sigma$. The result is in this case trivial, as the only eigenvalue with nonzero weight is $D_1 = \Gamma_\sigma/2 + i\omega_\sigma$ with weight $L_1 + iK_1 = 1$ purely Lorentzian. Note how including the complex weight in the computation of the complex energy spectrum allows to retain the one relevant resonance while the matrix M otherwise features four. As a conclusion, a 2LS excited incoherently is simply excited and release this excitation with the same energy by spontaneous emission, with a photoluminescence spectrum given by:

$$S(\omega) = \frac{1}{\pi} \frac{\Gamma_\sigma/2}{(\Gamma_\sigma/2)^2 + (\omega_\sigma - \omega)^2}. \quad (18)$$

There are no dynamical effects, shifts, dressing, renormalization of any sort. We now see how this changes considerably when upgrading the incoherent excitation to a coherent one.

The excitation of the 2LS by a coherent classical field, i.e., a c number $\Omega \exp(i\omega_l t)$ with Ω^2 the intensity of the driving laser, brings us to the Mollow master equation:

$$\partial_t \rho = i[\rho, \Omega(\sigma + \sigma^\dagger)] + \frac{\gamma_\sigma}{2} \mathcal{L}_\sigma \rho, \quad (19)$$

in the rotating frame and assuming that the 2LS and the laser are in resonance. Equation (19) yields the following matrix M :

$$M = \begin{pmatrix} 0 & -i\Omega & i\Omega & -\gamma_\sigma \\ -i\Omega & \gamma_\sigma/2 & 0 & i\Omega \\ i\Omega & 0 & \gamma_\sigma/2 & -i\Omega \\ 0 & i\Omega & -i\Omega & \gamma_\sigma \end{pmatrix}, \quad (20)$$

which has a more complex set of eigenvalues:

$$D_1 = 0, \quad (21a)$$

$$D_2 = \gamma_\sigma/2, \quad (21b)$$

$$D_\pm = \frac{1}{4} (3\gamma_\sigma \pm \sqrt{\gamma_\sigma^2 - 64\Omega^2}). \quad (21c)$$

The imaginary part of these quantities, that correspond to the energies of the transitions (real parts correspond to their broadening), are shown as a function of the intensity

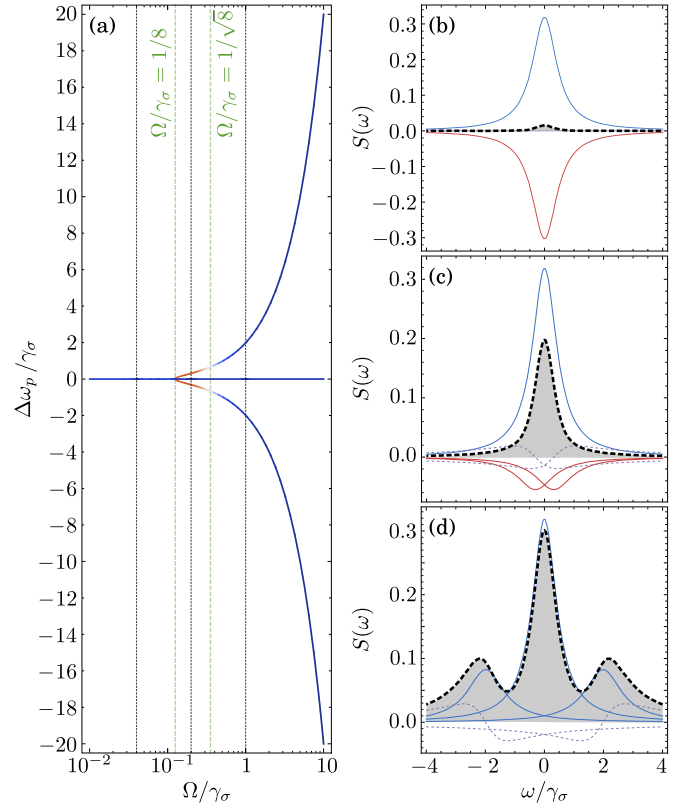


FIG. 2. Excitation by a coherent source. (a) Energy spectrum of a coherently driven 2LS. The energies that contribute to the total emission spectrum with positive Lorentzians are shown in blue, whereas those contributing as negative Lorentzians are shown in red. (b)–(d) Emission spectra of the target 2LS (dashed, black lines) for the values Ω/γ_σ marked by the vertical dashed lines in (a). The total emission spectrum is made of the sum of positive (blue lines) and negative (red) Lorentzians, and dispersive functions (dotted purple).

of the driving laser in Fig. 2(a). Their corresponding weight is encoded in the color: positive weights have blue shade while negative ones have a red shade.

This simple structure subtends a complex and rich phenomenology. At low intensity, $D_\pm \approx \gamma_\sigma(3 \pm 1)/4$ and the emission spectrum is as shown in Fig. 2(b), where D_2 is shown as the blue Lorentzian and D_- is shown as the red negative Lorentzian. The peak due to D_1 corresponds to the light scattered by the 2LS from the laser (not shown) and is known as the Rayleigh peak. This peak has zero linewidth, and is involved in the Heitler process that generates antibunched photons with the coherence of the driving laser [17].

In this case, and as long as $\Omega \leq \gamma_\sigma/8$, the spectrum consists of a single line as the eigenvalues' imaginary parts (that correspond to the states energies) are all degenerate. The combination of Eqs. (14) and (21) yields

$$S(\omega) = \frac{1}{2\pi} \frac{\gamma_\sigma/2}{(\gamma_\sigma/2)^2 + \omega^2} + \frac{1}{4\pi\beta} \frac{(3\gamma_\sigma - \beta)/4}{[(3\gamma_\sigma - \beta)/4]^2 + \omega^2} \frac{8(\beta + 5\gamma_\sigma)\Omega^2 - \gamma_\sigma^2(\gamma_\sigma + \beta)}{8\Omega^2 + \gamma_\sigma^2} + \frac{1}{4\pi\beta} \frac{(3\gamma_\sigma + \beta)/4}{[(3\gamma_\sigma + \beta)/4]^2 + \omega^2} \frac{8(\beta - 5\gamma_\sigma)\Omega^2 + \gamma_\sigma^2(\gamma_\sigma - \beta)}{8\Omega^2 + \gamma_\sigma^2}, \quad (22)$$

where $\beta = \sqrt{\gamma_\sigma^2 - 64\Omega^2}$. This total emission spectrum is shown with the black dashed line in Fig. 2(b) along with its decomposition into the underlying transitions (not splitted). The dressed states are largely compensating each other. This is the process of coherent absorption and reemission that endows this regime with peculiar properties. Besides, in this regime the light emitted by the 2LS is essentially coming from the Rayleigh peak (not shown). As a result of this structure of emission from the 2LS, the light emitted is antibunched and originates mainly from the Rayleigh peak, that has the first-order coherence of the laser (it is a δ peak for a c -number driving field). This is a strong feature of resonance fluorescence that has been observed by several groups [18–21]. It is counterintuitive as one would expect a scattered photon to retain also the second-order coherence of the laser, that is, to remain uncorrelated with other scattered photons. Note, however, that it would be incorrect to state that the scattered photons alone are antibunched. The effect is more subtle, and requires the coherent absorption and reemission process that originates from the compensating Lorentzian lines, even though the total intensity cancels out. Namely, filtering the emission to keep only the δ peak spoils the antibunching [22]. This is where lies the indeed counterintuitive characteristic of this emission: it requires the contribution of the incoherent fluorescence even though its intensity can be made vanishingly small! Our last assertion can be easily checked experimentally: the Rayleigh peaks from the same laser that excites two

two-level systems with different lifetimes will produce photons with different antibunching. For an ideal laser, both peaks are the same δ function. Yet, their antibunching is different, proof that some aspect of the incoherent fluorescence is involved, despite not explicitly in the power spectrum.

As far as strong coupling is concerned, the situation of interest is that of energy splitting between the dressed states. This occurs when:

$$\Omega > \gamma_\sigma/8, \quad (23)$$

and is shown in Figs. 2(a) and 2(c). Note that, strikingly, the splitted states have a negative weight, i.e., correspond to absorbing lines. While their position is consistent with the conventional dressed-state picture with energies $\omega_\pm = \pm\sqrt{64\Omega^2 - \gamma_\sigma^2}/4$, the dynamics involved is opposite to that of new states radiating at their corresponding energy. Instead, they enter the scene by absorbing energy. They start to emit light instead of taking it away for the more stringent condition [cf. Eq. (23)]:

$$\Omega > \gamma_\sigma/\sqrt{8}. \quad (24)$$

Figure 2(d) shows the emission spectrum for $\Omega = \gamma_\sigma$ with, in this case, an active contribution from all the dressed states that result in the characteristic emission spectrum as a triplet that is clearly understood from the dressed-state structure. In the limit of very large intensity, $D_\pm \approx 3\gamma_\sigma/4 \pm 2i\Omega$, and the emission spectrum is the well-known Mollow triplet [6]:

$$S(\omega) = \frac{1}{2\pi} \frac{\gamma_\sigma/2}{(\gamma_\sigma/2)^2 + \omega^2} + \frac{1}{4\pi} \frac{3\gamma_\sigma/4}{(3\gamma_\sigma/4)^2 + (\omega + \chi/4)^2} \left[\frac{8\Omega^2 - \gamma_\sigma^2}{8\Omega^2 + \gamma_\sigma^2} + \frac{\gamma_\sigma(40\Omega^2 + \gamma_\sigma^2)}{\chi(8\Omega^2 + \gamma_\sigma^2)} \left(\omega + \frac{\chi}{4} \right) \right] + \frac{1}{4\pi} \frac{3\gamma_\sigma/4}{(3\gamma_\sigma/4)^2 + (\omega - \chi/4)^2} \left[\frac{8\Omega^2 - \gamma_\sigma^2}{8\Omega^2 + \gamma_\sigma^2} - \frac{\gamma_\sigma(40\Omega^2 - \gamma_\sigma^2)}{\chi(8\Omega^2 + \gamma_\sigma^2)} \left(\omega - \frac{\chi}{4} \right) \right], \quad (25)$$

where $\chi = \sqrt{64\Omega^2 - \gamma_\sigma^2}$. The satellites contribute negatively to the total spectrum when they are close to the center, with effect of trimming the fat tails of the central Lorentzian. As a result, the system emits with a sharper distribution of frequencies, typically a Student- t distribution [that results from the difference of two Lorentzians, as shown in Fig. 2(b)]. This allows to collect more easily all the emitted photons in a narrower window of detection and as a result to achieve better values of antibunching. On the opposite, when the Mollow triplet is largely split, it consists of essentially three nonoverlapping Lorentzian lines (of linewidths $3\gamma_\sigma/4$ and γ_σ for the central and satellite peaks, respectively), its statistical properties recover those of an incoherently pumped 2LS. This understanding of the composition of the Mollow triplet, even before it is fully formed, is important not only on fundamental grounds, but also since it can be used to engineer better single-photon sources, as we will see in Sec. V.

D. Excitation by a single-photon source

In this and the following four sections, we upgrade the source of excitation from a classical to a quantum field. The

simplest quantum field is that provided by a single-photon source, which is modeled by an incoherently driven 2LS, as sketched in Fig. 1(a) with a thermal field (incoherent pumping) providing the classical excitation, and is described by Eq. (1) adding the Lindblad term $(P_\sigma/2)\mathcal{L}_{\sigma^\dagger\rho}$. The resulting Liouvillian matrix M has dimension 16×16 but only 4 of the 16 eigenvalues contribute to the steady-state emission spectrum. These eigenvalues are solutions to cubic equations that are too bulky to be written here. In Figs. 3(a)–3(i), we show the weighted energy spectrum of the target 2LS as a function of the intensity of the incoherent driving. For clarity, we split the positive (first column) and negative (second column) contributions that are shown together in the third column, with the same color code (blue, positive; red, negative). The upper row, Figs. 3(a)–3(c), shows the case where $\gamma_\xi/\gamma_\sigma = 0.1$ and the driving is too weak to dress the energies of the target 2LS: it behaves like its classical counterpart under incoherent pumping. Figures 3(d)–3(f) show the case where $\gamma_\xi/\gamma_\sigma = 1$, that results in a splitting of the energy levels, with a splitting that opens with absorbing lines before turning to emitting dressed states, as in the case of a 2LS driven by a coherent classical field. Unlike the latter, however, the splitting eventually quenches with increasing pumping rate. This can be

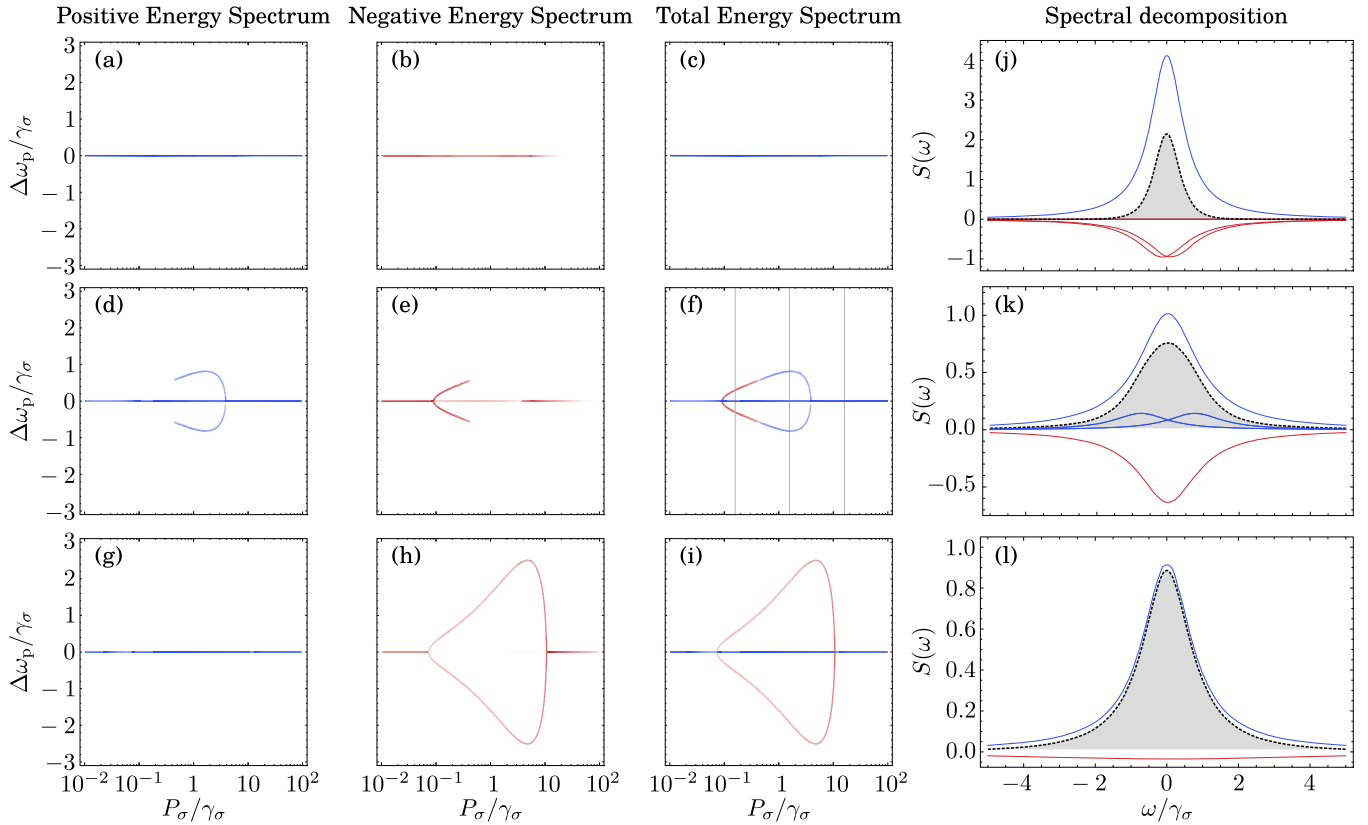


FIG. 3. Excitation by a single-photon source. (a)–(i) Energy spectra of the target 2LS. The energies that contribute to the total emission spectrum with positive Lorentzians are shown in blue, whereas those that contribute with negative Lorentzians are shown in red. (j)–(l) Emission spectra of the target 2LS (dashed, black lines) for the values P_σ/γ_σ marked by the vertical dashed lines in (f). The total emission spectrum is made of the sum of positive (blue lines) and negative (red lines) Lorentzians. To compute the figures, we set γ_σ as the unit, and set $\gamma_\xi/\gamma_\sigma = 0.1$ in (a)–(c), $\gamma_\xi/\gamma_\sigma = 1$ in (d)–(f), and $\gamma_\xi/\gamma_\sigma = 10$ in (g)–(i).

explained by the fact that the target 2LS is not driven efficiently in the high excitation regime since the emission spectrum of the source 2LS broadens [cf. Eq. (18)], reducing the intensity at the frequency of the target 2LS. In Fig. 3(f), we select three values for P_σ/γ_σ for which the total emission spectrum (dashed black line) is decomposed into its dressed-state emission (emitting in blue and absorbing in red), as shown in Figs. 3(j)–3(l). The magnitude of the Lorentzians at the splitted energies is not large enough to result in an observable splitting in the total

emission spectrum of the target 2LS. Figures 3(g)–3(i) show the case where $\gamma_\xi/\gamma_\sigma = 10$, with a third scenario of an energy splitting that occurs *only* with absorbing dressed states, but with a magnitude of the splitting that is larger than in the previous case. This case also fails to produce an observable splitting in the total luminescence spectrum. Even though the power spectrum remains a single peak throughout, one can still dress a 2LS with a SPS. The energy splitting of the target 2LS occurs when the following condition is satisfied:

$$\gamma_\xi/\gamma_\sigma \geq \left[\frac{P_\sigma^{*4} - 68P_\sigma^{*3} + 726P_\sigma^{*2} + 1 - 8\sqrt{-2P_\sigma^*(P_\sigma^{*2} - 16P_\sigma^* + 1)^3}}{P_\sigma^{*2} - 14P_\sigma^* + 1} \right]^{1/2}, \quad (26)$$

where we have introduced the unitless parameter $P_\sigma^* = P_\sigma/\gamma_\sigma$, and we note that the condition is valid only when the argument on the right-hand side of the inequality is a real value. The lower bound for P_σ^* is the real-valued zero that cancels the right-hand side of Eq. (26), which is the solution of a polynomial of order 8 for which we give a numerical approximation. When the right-hand side of Eq. (26) is real, it ranges from zero to infinity, which translates to a condition on the population of the source $0.93 \gtrsim n_\sigma \gtrsim 0.88$. Equation (26) thus provides the criterion for strong coupling of a 2LS with

the light emitted in the cw regime by a SPS. While this shows this is possible, with the source 2LS close to saturation, it also shows the conditions as required by the formula are not particularly enlightening. Since the complex energy spectrum remains (relatively) simple, one can go in this case one stage deeper and reconstruct from the resonances the structure of the dressed states.

The energy spectrum of a 2LS driven by a single-photon source, and the corresponding linewidths, are shown in Figs. 4(a) and 4(b), respectively. The black solid lines in

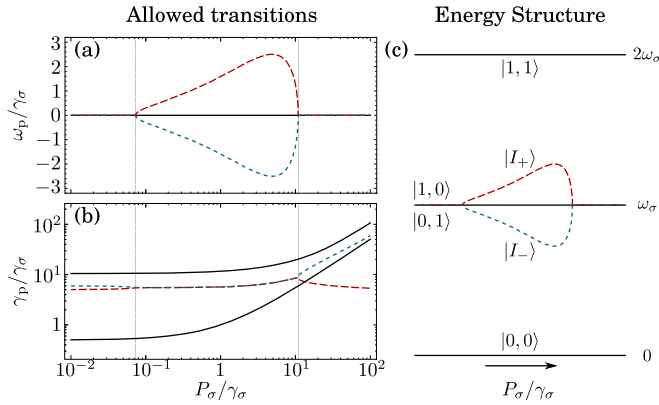


FIG. 4. Energy structure of a 2LS driven by a single-photon source. (a) Energy change due to the allowed transitions in the 2LS. (b) Linewidth of the emission of the 2LS for the allowed transitions. The transitions that involved the dressed states are shown by the dashed red and dashed blue lines. (a) Shows a splitting in the transition energies, while (b) shows that those transitions have the same linewidth. (c) The energy structure of the 2LS driven by a single-photon source is reconstructed from the allowed transitions in (a).

the figures correspond to transitions between the bare modes, i.e., from $|1\rangle_\sigma |1\rangle_\xi = |1,1\rangle$ to either $|1,0\rangle$ or $|0,1\rangle$, and from either $|1,0\rangle$ or $|0,1\rangle$ to $|0,0\rangle$. The blue and red dashed lines correspond to transitions involving dressed states that we note as $|I_\pm\rangle = \alpha|0,1\rangle + \sqrt{1-\alpha^2}e^{\pm i\phi}|1,0\rangle$, where $0 \leq \alpha \leq 1$. However, the appearance of the dressed states does not imply the absence of the bare state. On the contrary, they coexist giving rise to transitions from $|1,1\rangle$ to either $|I_+\rangle$ or $|I_-\rangle$, but only from $|0,1\rangle$ to $|0,0\rangle$: when the energy levels are splitted, the transition from $|1,0\rangle$ to $|0,0\rangle$ is suppressed as all the emission of the source 2LS is efficiently absorbed by the target 2LS, and instead takes place the coherent transfer from $|1,0\rangle$ to $|0,1\rangle$. Therefore, the schematic representation of the energy levels of a 2LS driven by a single-photon source is as shown in Fig. 4(c), where we show the coexistence of the bare and dressed states in the single-photon manifold.

E. Excitation by a Mollow triplet

In this section, we keep the same source 2LS but we excite it coherently. This systematic study of all the possibilities of exciting a 2LS by quantum light thus brings us to this curious configuration of exciting a 2LS with the Mollow triplet. The system is described by Eq. (1), using two input channels for the source with $\epsilon_1 = \epsilon_2 = \frac{1}{2}$, setting $H_\sigma = -i\sqrt{\epsilon_1\gamma_\sigma}\mathcal{E}(\sigma^\dagger - \sigma)$, and for simplicity we note $\Omega \equiv \sqrt{\epsilon_1\gamma_\sigma}\mathcal{E}$ as the intensity of the coherent light that drives the source 2LS. As in the previous section, the Hilbert space has dimension 16×16 , but in this case all the eigenvalues are involved in the energy spectrum of the target 2LS, as shown in Fig. 5 for several values of the ratio γ_ξ/γ_σ . The most obvious observation is the considerably higher complexity of the structure of the driven system. In this case, we will focus only on the resonances without making any attempt at reconstructing the underlying dressed states, as we did for the simplest configuration of exciting with a SPS. Figures 5(a)–5(c) show the case for $\gamma_\xi/\gamma_\sigma = 0.1$. The splitting also starts with absorbing states and occurs for a

driving intensity $\Omega/\gamma_\sigma \approx 0.02$, that is roughly one order of magnitude smaller than that required with a classical laser ($\Omega/\gamma_\sigma = \frac{1}{8}$). Other states do split at that usual threshold, showing that the target 2LS incorporates the energy structure of the source to its own. In fact, at large driving intensities, most of the energies converge to those of the source 2LS to provide a carbon copy of the conventional Mollow triplet (cf. Fig. 2). The most intense contributions to the total emission spectrum remain those provided by eigenvalues for which $|\Delta\omega_p/\gamma_\sigma| < 1$.

The total emission spectrum (dashed black lines) and its decomposition through dressed-states emission (blue and red solid lines) are shown in Figs. 5(j)–5(l) for the values of Ω/γ_σ marked by the vertical dashed lines in Fig. 5(c). Figure 5(j) displays another case of emergence of the dressed states as absorbing lines, besides, in this case, also strongly interfering with important dispersive components (dotted lines). As a result, the total spectrum broadens as compared to the simple target-2LS emission (blue line). Figure 5(k) shows how the dressed states now fully formed contribute to the emission with enough energy splitting and weight of the corresponding transition to produce a noticeable feature in the total emission spectrum (dotted black). However, negative contributions balance these peaks and the resulting emission spectrum only exhibits two “bumps” on its flanks. The target is resilient to developing a Mollow triplet, although its dressing is now unambiguous as observable directly in the luminescence. Figure 5(l) shows the quenching of the Mollow triplet at higher intensity of the source: the lateral peaks vanish and the remaining splitted energies lie close to the bare state, resulting in an emission spectrum with a single broad line.

Figures 5(d)–5(f) and 5(g)–5(i) show the energy spectrum of the target 2LS for $\gamma_\xi/\gamma_\sigma = 1$ and $\gamma_\xi/\gamma_\sigma = 10$, respectively. Although most of the features of the energy spectrum of the target 2LS remain when we increase its decay rate, a notable feature is observed when $\gamma_\xi/\gamma_\sigma = 1$: there appears in this case dressed states that are splitted in energy at all driving intensities, as seen in Fig. 5(e) for $\Omega/\gamma_\sigma < 10^{-1}$ through the asymptotic lines instead of the usual bifurcations. While the weights also vanish with decreasing driving intensity, they are never exactly zero and the structure of the dressed states is peculiar as they reveal themselves even at vanishing driving field intensity. This is another manifestation of how equal decay rates in coupled quantum-optical system lead to optimum strong-coupling conditions [23]. In this case, this opens a channel of excitation where the target 2LS can benefit from the strong coupling of the source 2LS (that is, in strong coupling from the strong classical driving field) regardless of its driving intensity. The information of strong coupling is therefore “encoded” in the photons emitted by the source and “restored” in the target. If the target and sources are different objects (due to mismatched decay rates), this information is lost.

F. Excitation by an incoherently driven cavity

In this and the following section, we change the source of excitation for a driven cavity. Here, we discuss the case of an incoherently driven cavity. The system is described by Eq. (1)

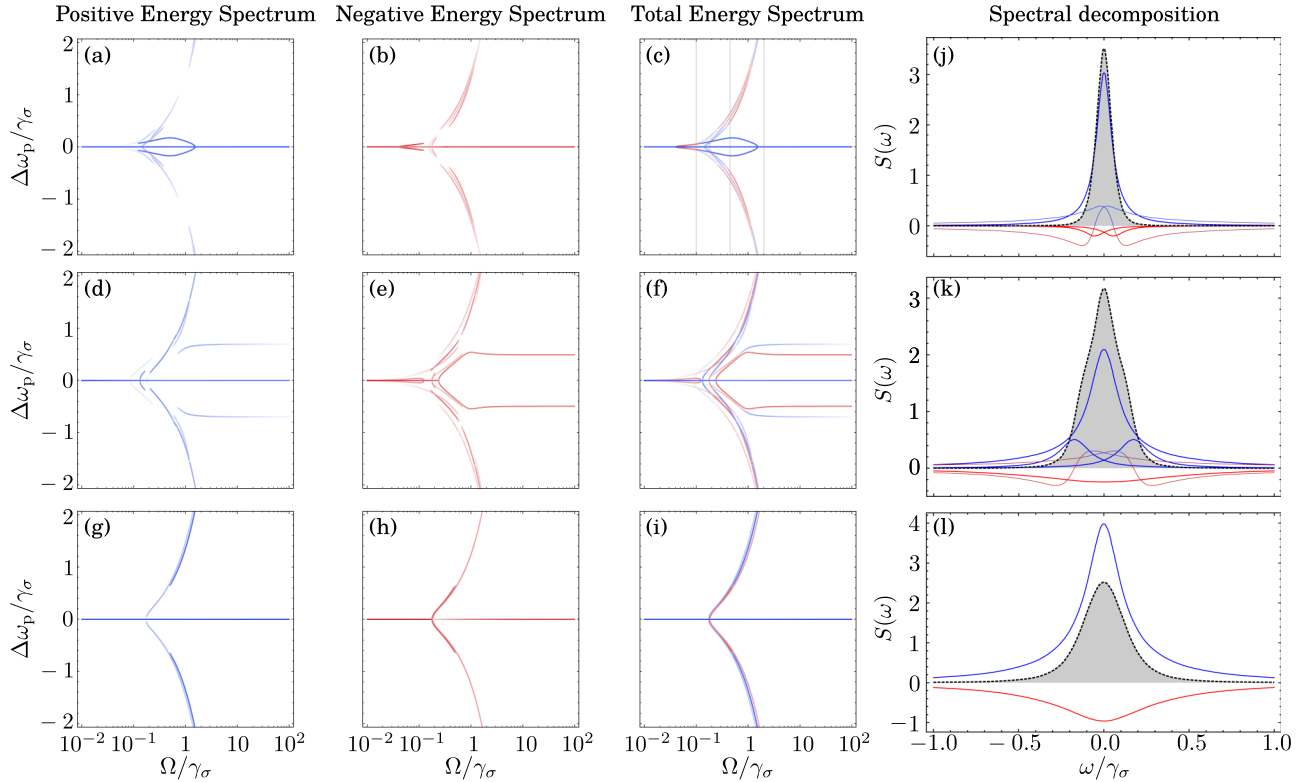


FIG. 5. Excitation by a Mollow triplet. (a)–(i) Energy spectra of the target 2LS. The energies that contribute to the total emission spectrum with positive Lorentzians are shown in blue, whereas those that contribute with negative Lorentzians are shown in red. (j)–(l) Emission spectra of the target 2LS (dashed, black lines) for the values Ω/γ_σ marked by the vertical dashed lines in (c). The total emission spectrum is made of the sum of positive (blue lines) and negative (red lines) Lorentzians. To compute the figures, we set γ_σ as the unit, and set $\gamma_\xi/\gamma_\sigma = 0.1$ in (a)–(c), $\gamma_\xi/\gamma_\sigma = 1$ in (d)–(f), and $\gamma_\xi/\gamma_\sigma = 10$ in (g)–(i).

when replacing the parameters of the source (operators and associated variables), marked with the subindex σ , by those corresponding to a cavity, which we note with the subindex a (the operator a is a boson annihilation operator). The incoherent driving of the cavity is described by the Lindblad term $(P_a/2)\mathcal{L}_a^\dagger\rho$ in the master equation. In contrast to the previous three sections, the Hilbert space of the system is now infinite. To compute the energy spectrum, we need to truncate in the number of excitations. This is a difficult constraint for an incoherently driven cavity since its population $n_a = P_a/(\gamma_a - P_a)$ has thermal fluctuations. For this reason, the energy spectra shown in Fig. 6 are computed up to $P_a/\gamma_a \approx 0.968$, with corresponding populations $n_a = 30$ for which we have checked convergence of the results. Figures 6(a)–6(c) display the case with $\gamma_\xi/\gamma_a = 0.1$ and show that the energy spectrum is qualitatively similar to a 2LS driven by a classical laser [cf. Fig. 2(a)]. The most notable features of this result are the following: first, weighting the transitions in a truncated Hilbert space is mandatory to reach convergence, as D_p alone do not yield a stable structure otherwise as not only the number of eigenvalues grows with the size of truncation, but their distribution also fails to settle to a consistent pattern. Second, the weighted complex energy spectrum, shown in Fig. 6, that is well defined and for which we have checked convergence, reduces to a simple structure in the spectral shape but still exhibits some unexpected features, namely, up to three satellite energies visible on each flank of the central Lorentzian, as compared to the single

line of the conventional Mollow triplet [cf. Fig. 2(a)]. The system fluctuates so much that it cannot accommodate all the transitions with three energies only. Third, while the weighted structure is indeed similar to the classical excitation, the intensity of the satellite peaks is much smaller in comparison, so that the total emission spectrum is barely affected by them and is given essentially by a single Lorentzian at the energy of the target 2LS, as shown in Figs. 6(g) and 6(h) for the values P_a/γ_a marked by the vertical dashed lines in Fig. 6(c). The excitation of a 2LS by thermal light is therefore largely a case of fundamental interest that, for most purposes, can be approximated to an incoherently excited 2LS, despite this configuration yields a dressing of the target. Fourth, as in the previous case, setting the decay rate of the target 2LS equal to the decay rate of the cavity leads to energy splitting at all values of pumping, while a mismatch leads to a bifurcation instead, as shown in Figs. 6(d)–6(f). In summary for this configuration, there is little physics in the main observable, but much to be learned on the mechanisms of quantum excitation from a (quantized) thermal source.

G. Excitation by a coherently driven cavity

In this section, we describe the energy splitting of a 2LS driven by the emission of a coherently driven cavity. The system is described by Eq. (1) with the changes of the previous section, but now we use two input channels for the source with $\epsilon_1 = \epsilon_2 = \frac{1}{2}$, we replace the incoherent pumping of

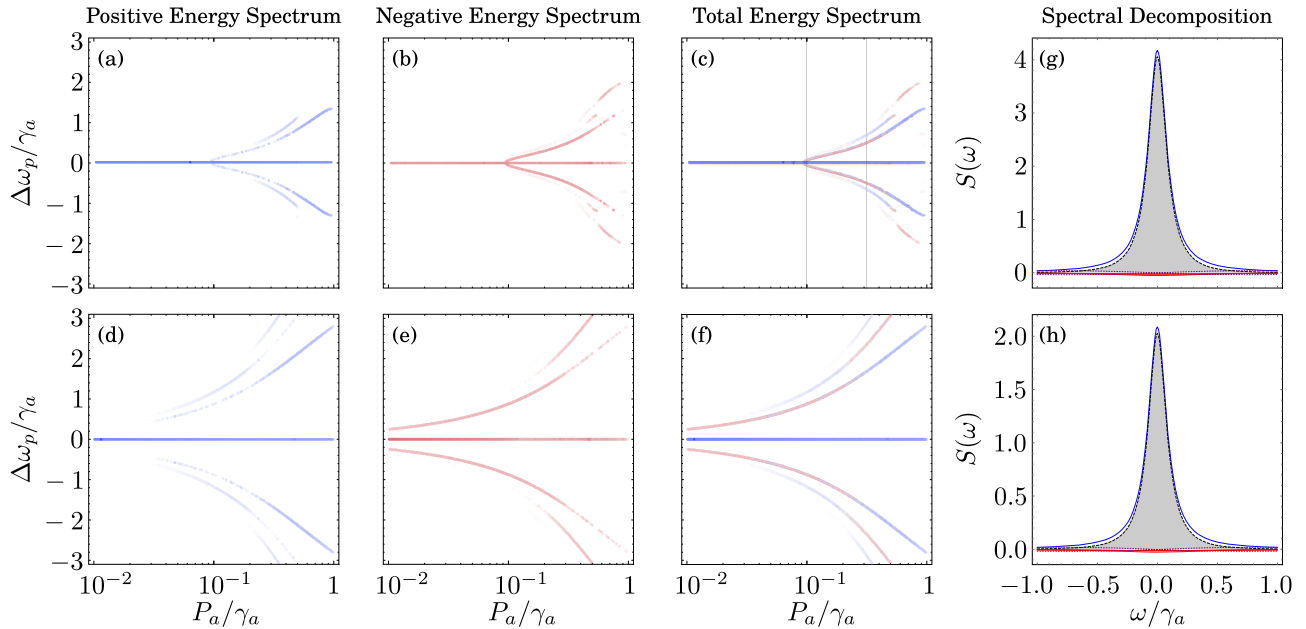


FIG. 6. Excitation by an incoherently driven cavity. (a)–(f) Energy spectra of the target 2LS. The energies that contribute to the total emission spectrum with positive Lorentzians are shown in blue, whereas those that contribute with negative Lorentzians are shown in red. (g), (h) Emission spectra of the target 2LS (dashed, black lines) for the values P_a/γ_a marked by the vertical dashed lines in (c). The total emission spectrum is made of the sum of positive (blue lines) and negative (red lines) Lorentzians. To compute the figures, we set γ_a as the unit, and set $\gamma_\xi/\gamma_a = 0.1$ in (a)–(c), and $\gamma_\xi/\gamma_a = 1$ in (d)–(f).

the source by $H_a = -i\sqrt{\epsilon_1\gamma_a}\mathcal{E}(a^\dagger - a)$, and set the effective driving intensity of the source as $\Omega = \sqrt{\epsilon_1\gamma_a}\mathcal{E}$. This creates a coherent state $|2\Omega/\gamma_a\rangle$ that is dynamically coupled to the 2LS. The dimension of the Hilbert space is also infinite and must be truncated. In this case, however, Poissonian fluctuation of the cavity makes the truncation manageable up to large populations.

The energy spectrum of the target 2LS is shown in Figs. 7(a)–7(c) for $\gamma_\xi/\gamma_a = 0.1$ and in Figs. 7(d)–7(f) for $\gamma_\xi/\gamma_a = 1$. The notable features here are direct counterparts of the incoherent excitation case: First, the weighted energy spectrum now fully reduces to the level of complexity of the conventional Mollow triplet, with exactly three resonances. Here, it must be borne in mind that the underlying structure is that of a fully quantized 2LS cavity system, with countably infinite complex eigenvalues (that fail to provide a converged structure if unweighted). In the Hamiltonian regime, the corresponding structure is extremely complicated [12] and this is the cascaded feature (of no feedback from the target to its source) that brings such a simplification with an actual triplet structure down to the most fundamental level. This is not exactly the conventional Mollow case, however, since there is one additional parameter, the decay rate of the cavity γ_a , that cannot be zero as otherwise no photons are emitted by the source. This causes some differences between these two configurations: the c -field on the one hand and the coherent-state cavity on the other. Figure 7 shows two cases for the latter with different γ_ξ/γ_a . Interestingly, in this case, the configuration $\gamma_a = \gamma_\xi$ does not lead to an asymptotic loss of the splitting but to a bifurcation. This splitting from a single line always occurs before that of the conventional Mollow triplet. The energy spectra remain qualitatively very similar

to that of the c -field driving (cf. Fig. 2). The agreement is recovered at large drivings where a mean-field approximation, that replaces the cavity operator a by $\sqrt{n_a}$ in Eq. (1), converges to the numerical solution. This approximation leads to the master equation of a 2LS driven by a laser with intensity $\Omega^* = \sqrt{(1 - \epsilon_1)\gamma_\xi\gamma_a n_a} = \sqrt{\gamma_\xi\gamma_a n_a/2}$ so the agreement at large Ω (where n_a is very large too) appears to be exact. The mean-field approximation does not hold, however, for small values of Ω/γ_a and therefore fails to predict the splitting threshold. In this case, strong correlations between the 2LS and the few photons from the quantized driving field (albeit in a coherent state) exist that lead to differences from the c -field driving. We come back to their importance in the last part of the paper, Sec. V, where we turn to applied considerations of this physics.

H. Excitation by a one-atom laser

In this section, we consider an actual laser as the source for the 2LS. Namely, we drive the 2LS with the coherent state generated by a device that creates this coherence from its internal dynamics, without inheriting it from another classical source (e.g., another laser, a classical field, etc.) This is the culminating point of our description of the Mollow physics in this text as there is no bad approximation that causes unphysical and/or pathological results, which could come from the δ peak of the laser [22]. There have been several efforts to go beyond the Mollow paradigm where the driving light is a perfect sine wave, for instance, Zoller's earliest work (that was the topic of his Ph.D. thesis) [24–26], where the sought features of the driving field are enforced into the model. Here, in line with the cascaded formalism philosophy, we leave to

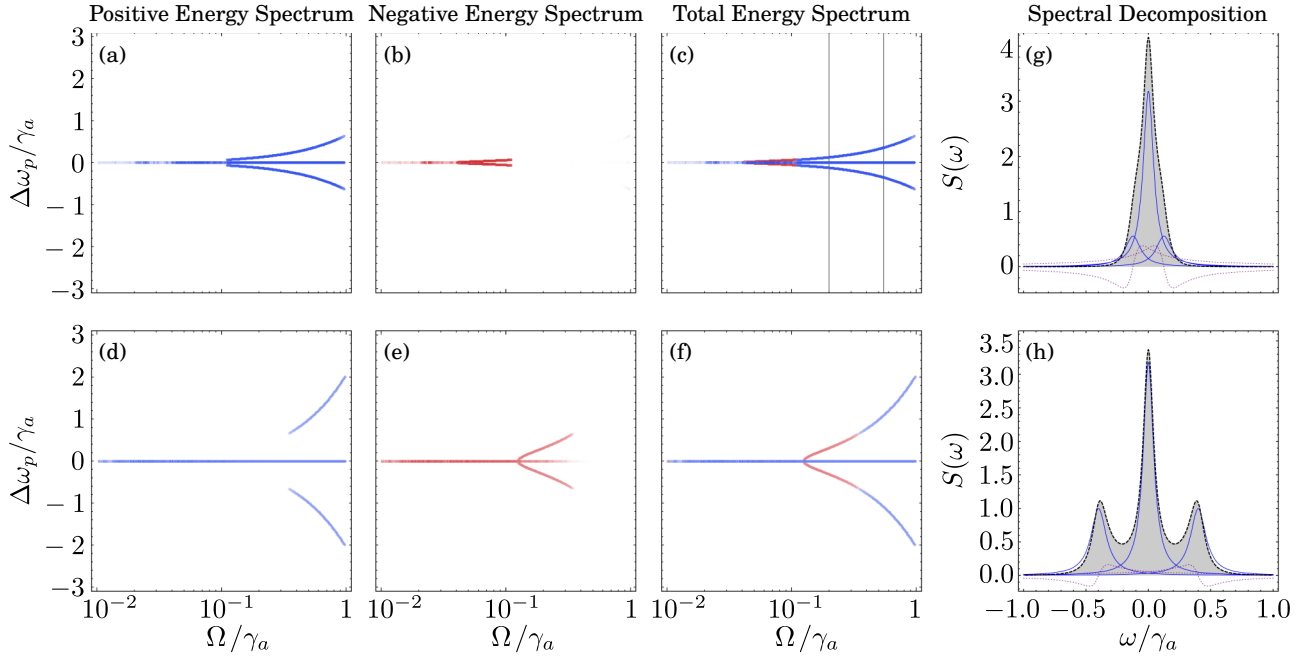


FIG. 7. Excitation by a coherently driven cavity. (a)–(f) Energy spectra of the target 2LS. The energies that contribute to the total emission spectrum with positive Lorentzians are shown in blue, whereas those that contribute with negative Lorentzians are shown in red. (g), (h) Emission spectra of the target 2LS (dashed, black lines) for the values Ω/γ_σ marked by the vertical dashed lines in (c). The total emission spectrum is made of the sum of positive (blue lines) and negative (red lines) Lorentzians. To compute the figures, we set γ_a as the unit, and set $\gamma_\xi/\gamma_a = 0.1$ in (a)–(c), and $\gamma_\xi/\gamma_a = 1$ in (d)–(f).

the source to self-consistently develop and establish its lasing properties. The simplest such laser is the one-atom laser [27], that is able to turn an incoherent pumping of the 2LS into a coherent state of the cavity [28–30]. Its Hamiltonian is that of Jaynes and Cummings [9]:

$$H_s = \omega_\sigma \sigma^\dagger \sigma + \omega_a a^\dagger a + g(a^\dagger \sigma + \sigma^\dagger a), \quad (27)$$

where, as before, σ is the fermionic operator describing the atom and a is the bosonic operator describing the cavity, with respective free energies ω_σ and ω_a . Now, however, they are coupled reversibly with strength g . The incoherent driving of the atom (P_σ), the decay processes, and the cascaded coupling between the cavity and the target 2LS are included in the master equation:

$$\begin{aligned} \partial_t \rho = & i[\rho, H_s + H_\xi] + \frac{P_\sigma}{2} \mathcal{L}_{\sigma^\dagger} \rho + \sum_{k=\{\sigma, a, \xi\}} \frac{\gamma_k}{2} \mathcal{L}_k \rho \\ & + \sqrt{\gamma_a \gamma_\xi} \{[a \rho, \xi^\dagger] + [\xi, \rho a^\dagger]\}. \end{aligned} \quad (28)$$

Here, γ_σ , γ_a , and γ_ξ are the decay rates of the atom inside the cavity, the cavity, and the target 2LS, respectively; and since there is no external coherent field driving the system we consider only one input channel for the source and for the target. In Fig. 8, we show the normalized emission spectra of a 2LS cascaded by a one-atom laser (solid lines), and we compare it to the normalized emission spectra of a 2LS driven by a classical laser (dashed lines). In the bottom three lines of Fig. 8, the incoherent driving of the atom is so small that the one-atom laser is not in the lasing regime. Therefore, the comparison of the spectra is made so that the population in the target 2LS and in the coherently driven 2LS are the same. In all the other cases, when the one-atom laser is in the lasing

regime, the comparison of the spectra is made so that the driving intensity is the same, i.e., we compare the spectra of the target 2LS with that of a 2LS driven coherently with intensity $\Omega^* = \sqrt{\gamma_\xi \gamma_a n_a}$, where n_a is the population of the cavity. Figure 8 shows neatly the splitting of the energy levels of the target 2LS as a function of the rate of incoherent driving of the atom inside the cavity. At the lowest P_σ , the spectrum of the target 2LS is the one at the left bottom part of the figure. There, we see clearly that the target 2LS is acting as filter of the emission of the cavity: the central peak corresponds to the resonance of the target 2LS, while the other two peaks reveal the Rabi doublet due to the strong coupling between the cavity and the atom inside. As the incoherent driving of the atom increases, the peaks corresponding to the Rabi doublet become less dominant, and the emission spectrum of the target 2LS tends to merge into a broad single line. Increasing even further the incoherent driving, the emission line of the target 2LS begins to split again, but in a different way than the coherently driven 2LS: while the splitting of the target 2LS seems to be a doublet as, e.g., in the light green line, the spectrum of the coherently driven 2LS has clearly a triplet shape. At large driving rates, the emission of the target 2LS converges to that of the coherently driven 2LS. In fact, in the uppermost spectrum, the cavity has 100 photons, its statistics is coherent (that is $\langle a^\dagger a^\dagger a a \rangle / n_a^2 = 1$), and the two spectra are exactly the same in their fluorescence spectrum. The Rayleigh scattering peak, not shown for the conventional Mollow triplet (it is a δ function) arises in the other case as a very sharp luminescence line, as seen in the inset of Fig. 8.

In Fig. 9, we show a density plot of the photoluminescence spectrum of the target 2LS driven by all the sources of light

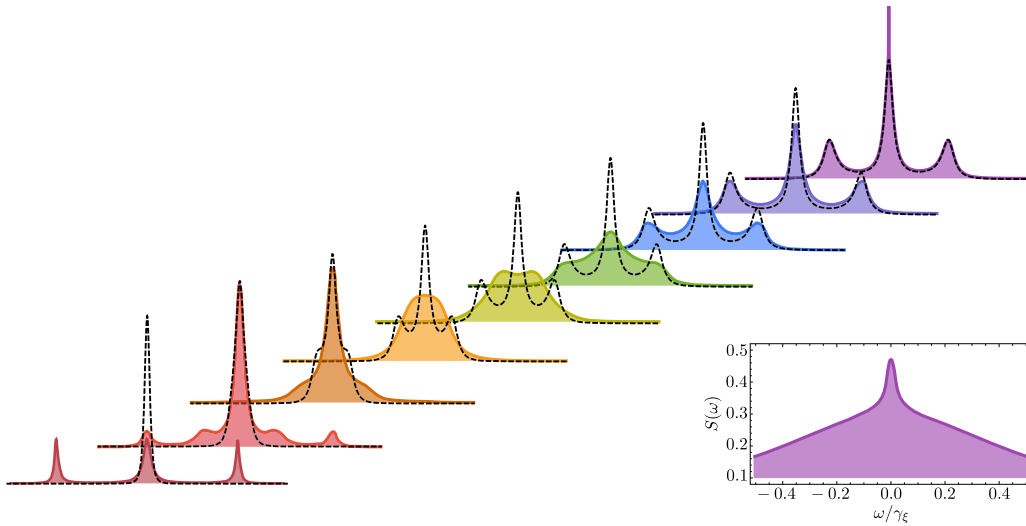


FIG. 8. Dressing of the target 2LS with a one-atom laser. We compare the normalized emission spectra of a 2LS driven by the emission of a one-atom laser (solid color lines) with the normalized emission spectra of a 2LS driven coherently by a classical laser (dashed black lines). The incoherent driving of the one-atom laser increases towards the upper right corner of the figure, and makes the emission spectra of the target 2LS to change from a filter of the emission of the cavity, as is clear from the lateral peaks due to the strong coupling between the cavity and the atom inside, to the splitting of the emission line until it reaches a triplet shape equivalent to that of a coherently driven 2LS. To compute the figures, we set the atom, the cavity, and the target 2LS in resonance, and the rest of the parameters were as follows: γ_x was set as the unit, $\gamma_\sigma/\gamma_x = 10^{-2}$, $\gamma_a/\gamma_x = 1$, $g/\gamma_x = 10$. The incoherent driving rate P_σ is different for each spectrum; for the spectrum at the bottom we took the limit $P_\sigma/\gamma_x \rightarrow 0$. For the next seven lines we used the P_σ such that $\Omega/\gamma_x = \sqrt{\gamma_a \gamma_x n_a}/\gamma_x = 0.5, 1.0, 1.5, 2.0, 2.5, 3.0$, and 3.5 . The last spectrum, at the top right of the figure, was obtained for a cavity with $\gamma_a/\gamma_x = 0.1$ and $P_\sigma/\gamma_x = 20.115$, so that the population in the cavity was 100 photons. The inset shows a zoom on this last spectrum very close to the resonance of the target 2LS, to show the Rayleigh peak due to the driving by the laser.

that we have considered in this section, which are summarized in its caption. In the next Section, we turn to more practical considerations and discuss how to bring such effects to useful applications.

V. CASCADED SINGLE-PHOTON SOURCES

Cascading is a powerful concept that allows to achieve extremely high end values from a moderate initial input, with such compelling examples as the domino effect [31] that can amplify energy by over 2×10^9 in a basement, to trophic cascade [32] that can lead to extinction of species. It acts in several key processes of various areas of science, e.g., with

chemical [33] and nuclear [34] chain reactions. In optics, through stimulated emission, it underpins basic phenomena such as superradiance [35] and lasing [36]. With the advent of heterostructures, it became possible to engineer more elaborate schemes to better control the chain reaction. A highlight is the proposal by Kazarinov and Suris of energy staircases in a superlattice leading to the successive creation of an increasing number of photons by a single initial electron [37], a scheme realized a quarter of a century later under the name of a quantum cascade laser [38]. Recently, another proposal was made with cascades between condensates [39] and extremely high correlations in the form of superbunching were shown to occur as a result of the cascading [40].

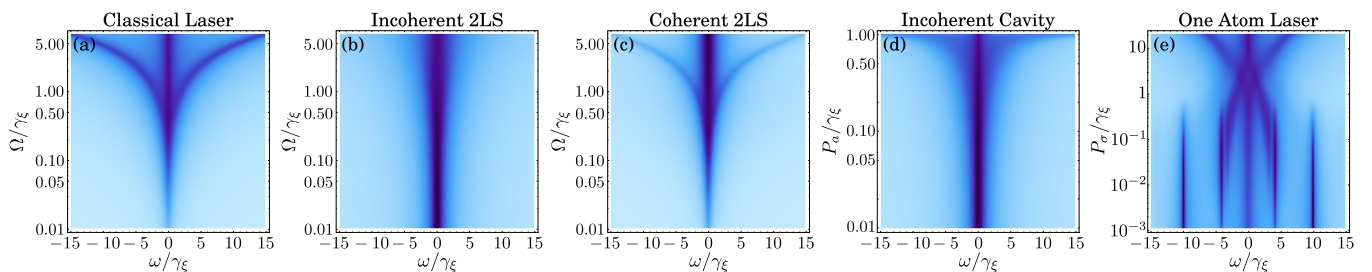


FIG. 9. Photoluminescence spectra of the two-level system driven by all the sources studied in the text. (a) A classical laser resulting in the conventional Mollow triplet. (b) An incoherent 2LS providing a single line that merely broadens. (c) A coherent 2LS providing a Mollow splitting but of weak intensity and that vanishes with increasing driving intensity. (d) A thermal cavity providing a single line whose broadening is reminiscent of the Mollow structure. (e) A one-atom laser showing the transition from the nonlasing regime of the driving source to the exact recovering of the conventional Mollow triplet. At low driving, the target echoes the structure from a Jaynes-Cummings-type coupling with the source.

A. Driving the cascaded SPS

In this section, we propose the application of such a principle to quantum light, and with the aim of increasing not the intensity of light, but a quality dear to quantum engineers, namely, the suppression of multiple-photon emission, known as antibunching [41]. This goal is highly pursued to power quantum information processing, with boson sampling [42]—not the most useful but the most accessible demonstration of quantum parallelism out of the classical reach—already in sight provided one could power linear optical setups with slightly better SPS. For this reason, there is a race to build always better sources, in particular in the semiconductor community where such devices would furthermore have a large economic and technological potential [43–45]. The Fourier transform limit for single-photon emission has already been reached [46] and there are now many efforts to combine and enhance other features such as brightness, efficiency, and, of course, antibunching [47–49]. Our proposal takes a different direction and rather than bettering engineering and implementation, we turn to a different mechanism to increase the quality of SPS by magnitudes not accessible only with a better technology. Namely, we propose to cascade the output of a chain of single-photon sources (SPS), with effect of a profound restructuring of their spectral emission, bringing the initial Lorentzian shape of a single SPS to grow into a Student- t line shape of order $2k$ after k iterations of the cascade. We show that such a spectral engineering that trims the fat Lorentzian tails is accountable for increased antibunching. As the iterations converge towards a normal distribution, our scheme allows to engineer extremely antibunched single-photon sources that could power quantum logic with the repetition rates necessary for their successful operations at a large scale. In essence, our results remove the constraint of spectral broadening associated to short lifetimes. Stated otherwise, it achieves at the single-photon emission level what a laser does in the Schallow-Townes limit by narrowing the line with increasing signal.

Our proposal consists of an array of consecutive SPS, in which the first SPS is excited externally while the rest of them are excited by the fluorescence of the previous SPS. We will consider cascades of up to three emitters but the scheme can be continued indefinitely. The underlying principle is that exciting with quantum light allows to access new regimes that neither classical excitations nor reversible (Hamiltonian) coupling can provide [5]. This is thanks to the added degrees of freedom of quantum light on the one hand (such as reduced fluctuations) and the one-way transfer of energy on the other hand that removes the effective decay implied by strong-coupling oscillating the excitation back to its source.

Here, more than in the other cases discussed so far, a fully integrated approach might be desirable to realize a device. The scheme consists in feeding the output field of the i th system to the input field of the $(i + 1)$ th system, with no feedback. This could be achieved by unidirectional couplers in the laboratory or, as already commented in Paper I [5], by using chiral waveguides to assemble the whole architecture compactly on the same chip [50,51]. It could also be possible to use a highly directional source of excitations [52] or a direct

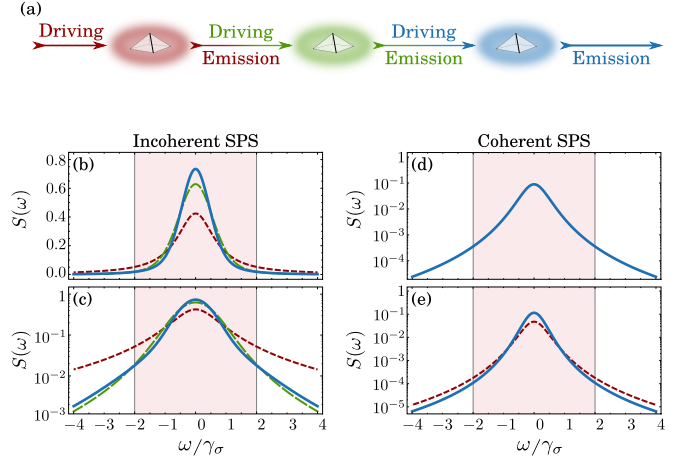


FIG. 10. Scheme of the cascaded single-photon sources. (a) A series of SPS is connected through a cascaded architecture. In each step of the cascade, a SPS is driven by the emission of the previous SPS. (b)–(d) Emission spectra of the initial SPS (red, dotted), the first (green, dashed), and second (blue, solid) cascade steps. In each step of the cascade, the emission line becomes narrower and more peaked around the central frequency. Panels (b) [linear scale] and (c) [log scale] were made with $\gamma_g/\gamma_\sigma = P_\sigma/\gamma_\sigma = 1$. In Panel (d), the coherent driving excites all the SPS in the cascade while in Panel (e), it drives only the first SPS. In both cases, each SPS drives the next one with its fluorescent output.

photonic coupling [53]. A schematic representation is shown in Fig. 10(a) and reads as follows: the first SPS is driven by an external pumping, and the emission of SPS1 is then sent to SP2, and so on and so forth as more stages of the cascade are arranged. An array of N SPS with annihilation operators σ_i , Hamiltonian H_i , and decay rate γ_i can then be described by a master equation in the form [54]:

$$\begin{aligned} \partial_t \rho = & \sum_{j=1}^N \left(i[\rho, H_j] + \frac{\gamma_j}{2} \mathcal{L}_{c_j} \rho - \sqrt{\gamma_j} [\mathcal{E} c_j^\dagger - \mathcal{E}^* c_j, \rho] \right) \\ & + \sum_{j=2}^N \sum_{l=1}^{j-1} \sqrt{\gamma_j \gamma_l} \{ [c_l \rho, c_j^\dagger] + [c_j, \rho c_l^\dagger] \} + \frac{P_{c_1}}{2} \mathcal{L}_{c_1} \rho, \end{aligned} \quad (29)$$

where \mathcal{E} is the amplitude of the coherent field incident upon SPS1. The justification for this master equation is given in the Appendices A and B, and we have featured explicitly an incoherent pumping of the first SPS at the rate P_{c_1} , that can be set to zero to consider the effect of the coherent driving only. The antibunching of a two-level system is, ideally, exactly zero. An actual experiment will detect two photons even in absence of noise and extraneous emitters, from the SPS itself. This is due to time uncertainty that can bring together two photons close enough in time to exhibit photon bunching. For some fixed-time unit set by the detector, the larger the emission rate, the more likely are such spurious coincidences. In the frequency space, this is linked to tail events that are not detected, for instance, because the detector’s bandwidth Γ is finite. Accordingly, while detecting all photons at all frequencies, $\Gamma \rightarrow \infty$, produces the ideal

$g_\infty^{(2)}(\tau = 0) = 0$, failure to do so results in bunching [55]. The fastest is the source, the broader is the spectrum and the more difficult it becomes to collect all the photons. Crucially, the spectrum is a Lorentzian and consequently has fat tails. This means that outliers are frequent, unlike a normal distribution where they are exponentially suppressed until they become completely negligible. A fat-tail distribution can never safely exclude all its outliers, regardless of the filters' bandwidth. There would therefore appear to be an intrinsic limitation between emission rate and photon antibunching. We now show how to thwart such a predicament by trimming the fat tails. Figure 11 shows the combined emission rate and antibunching $g_\Gamma^{(2)}$ for a SPS that is excited either incoherently (solid red) or coherently (solid black) as pumping is varied (dummy parameter on the curve). This figure is for a detector

bandwidth $\Gamma = 4\gamma_\sigma$. Increasing Γ , one both better the emission rate and antibunching, towards their ideal values of γ_σ and 0, respectively. However, this is a slow convergence that requires unpractical large filters at a disadvantage with the fat Lorentzian tails. The exact functions of Γ and other parameters are given by, in the case of incoherent pumping at rate P_σ :

$$I_\sigma^{\text{inc}} = \gamma_\sigma P_\sigma / (\gamma_\sigma + P_\sigma) \int_{-\Gamma/2}^{\Gamma/2} S(\omega) d\omega, \quad (30a)$$

$$g_\sigma^{(2),\text{inc}} = \frac{2}{1 + 3 \tan[\pi(\gamma_\sigma + P_\sigma) I_\sigma^{\text{inc}} / (2\gamma_\sigma P_\sigma)]}, \quad (30b)$$

where Eq. (30b) is valid for $I_\sigma^{\text{inc}} \leq \gamma_\sigma P_\sigma / (\gamma_\sigma + P_\sigma)$. The coherent counterpart is given by:

$$I_\sigma^{\text{coh}} = \frac{4\gamma_\sigma \Omega^2}{\gamma_\sigma^2 + 8\Omega^2} \int_{-\Gamma/2}^{\Gamma/2} S(\omega) d\omega, \quad (31a)$$

$$g_\sigma^{(2),\text{coh}} = \left\{ 2\gamma_{\tilde{1}\tilde{1}}(\gamma_{0\tilde{1}}^2 + 8\Omega^2)(\gamma_{\tilde{1}\tilde{1}}\gamma_{\tilde{2}} + 16\Omega^2)[\gamma_{\tilde{1}\tilde{1}}^2\gamma_{\tilde{2}\tilde{1}}\gamma_{\tilde{3}\tilde{1}}\gamma_{\tilde{2}}\gamma_{\tilde{3}\tilde{2}}(9\gamma_{\tilde{1}\tilde{0}}^2 + 7\gamma_{\tilde{1}\tilde{0}}\gamma_{\tilde{0}\tilde{1}} + \gamma_{\tilde{0}\tilde{1}}^2) + 4\gamma_{\tilde{1}\tilde{1}}\gamma_{\tilde{3}\tilde{2}}(84\gamma_{\tilde{1}\tilde{0}}^4 + 16\gamma_{\tilde{1}\tilde{0}}^3\gamma_{\tilde{0}\tilde{1}} + 118\gamma_{\tilde{1}\tilde{0}}^2\gamma_{\tilde{0}\tilde{1}}^2 + 31\gamma_{\tilde{1}\tilde{0}}\gamma_{\tilde{0}\tilde{1}}^3 + 2\gamma_{\tilde{0}\tilde{1}}^4)\Omega^2 + 32\gamma_{\tilde{1}\tilde{0}}(51\gamma_{\tilde{1}\tilde{0}}^3 + 75\gamma_{\tilde{1}\tilde{0}}^2\gamma_{\tilde{0}\tilde{1}} + 38\gamma_{\tilde{1}\tilde{0}}\gamma_{\tilde{0}\tilde{1}}^2 + 8\gamma_{\tilde{0}\tilde{1}}^3)\Omega^4 + 768\gamma_{\tilde{1}\tilde{0}}^2\Omega^6] \right\} / \left\{ 3\gamma_{\tilde{3}\tilde{1}}(\gamma_{\tilde{1}\tilde{1}}\gamma_{\tilde{2}\tilde{1}} + 4\Omega^2)(\gamma_{\tilde{1}\tilde{1}}\gamma_{\tilde{2}\tilde{1}} + 8\Omega^2)(\gamma_{\tilde{3}\tilde{1}}\gamma_{\tilde{3}\tilde{2}} + 16\Omega^2)(\gamma_{\tilde{1}\tilde{1}}\gamma_{\tilde{2}\tilde{1}} + 8\gamma_{\tilde{1}\tilde{0}}\Omega^2)^2 \right\}, \quad (31b)$$

where we have used again the compact notation $\gamma_{nm}^k = (n\Gamma + m\gamma_\sigma)^k$. From these results, and as is apparent in Fig. 11, the coherent driving provides better antibunching than its incoherent counterpart, with plateaus of $g_\sigma^{(2),\text{coh}} = 2\gamma_{0\tilde{1}}^2(9\gamma_{\tilde{1}\tilde{0}}^2 + 7\gamma_{\tilde{1}\tilde{0}}\gamma_{\tilde{0}\tilde{1}} + \gamma_{\tilde{0}\tilde{1}}^2)/3\gamma_{\tilde{1}\tilde{1}}^2\gamma_{\tilde{2}\tilde{1}}\gamma_{\tilde{3}\tilde{1}}$ and $g_\sigma^{(2),\text{inc}} = 2\gamma_{\tilde{0}\tilde{1}}/\gamma_{\tilde{3}\tilde{1}}$, which for $\Gamma = 4\gamma_\sigma$ reduce to $346/8775 \approx 0.039$ and $2/13 \approx 0.154$, respectively. The maximum emission rate, however, is smaller. This is due to stimulated emission induced by the coherent driving that Rabi oscillates back the excited state to the ground state and thus saturates the SPS to at most half its full occupancy. In contrast, the incoherent driving can saturate the two-level system to its excited state and can thus emit twice as much. The reason for a better antibunching of the coherent driving has already been discussed above in the context of the Heitler effect. It is related to the spectral shape that trims its fat tails by destructive interferences. In the case of the Mollow triplet, we have shown above that it consists of three Lorentzians centered at $\omega = 0$, and $\omega = \pm\sqrt{64\Omega^2 - \gamma_\sigma^2}$ as shown in Eq. (25). In the limit of vanishing driving, the resulting line shape thus concentrates its emission to the central peak with a distribution of the type:

$$S(\omega) = \frac{1}{\pi} \frac{32\gamma_\sigma \Omega^2}{(\gamma_\sigma^2 + \omega^2)^2}, \quad (32)$$

which is proportional to a Student- t distribution of order 3. The tails of this distribution vanish faster than those of a Lorentzian distribution. A given frequency window collects more photons from the SPS and its antibunching is therefore more like that of the full spectrum, that provides the exact zero.

We can extend this principle to cascaded systems, where the driving of the SPS is not from an external classical laser

(which, since it does not get feedback, can be seen as a particular case of cascading) but from another 2LS. For the case of incoherent pumping, we observe a similar behavior in the emission spectrum, as a difference of Lorentzians leads to a distribution with faster decaying tails. Namely, the emission spectrum of the first cascade reads, at vanishing pumping:

$$S_\xi(\omega) = \frac{1}{2\pi} \frac{\gamma_\sigma \gamma_\xi}{\gamma_\xi - \gamma_\sigma} \left[\frac{1}{(\gamma_\sigma/2)^2 + \omega^2} - \frac{1}{(\gamma_\xi/2)^2 + \omega^2} \right] = \frac{2}{\pi} \frac{\gamma_\sigma \gamma_\xi (\gamma_\sigma + \gamma_\xi)}{(\gamma_\sigma^2 + 4\omega^2)(\gamma_\xi^2 + 4\omega^2)}, \quad (33)$$

which is a Student- t distribution of order 3. In the next stage in the cascade, the resulting distribution is a Student t of order 5.

There is a tradeoff between the antibunching and the intensity of the emission of the cascaded single-photon source. The improvement of the value of $g_\Gamma^{(2)}$ is maximum when all the SPS have the same decay rate. In Fig. 11, we show the antibunching as a function of the emission rate of the cascaded SPS at various steps of the cascade, and for both the coherent and the incoherent driving. The coherent (solid, black line) and incoherent (solid, red line) are simply a SPS driven by a classical field. In the first step of the cascade, we obtain a large enhancement in the antibunching: for a wide range of intensities, the antibunching for the first step in the incoherent cascade (dotted, green line) matches the antibunching obtained with the coherent SPS, which shows again how driving a system with a classical laser can be seen as cascade. On the other hand, the antibunching for the first step in the coherent cascade (dashed, orange line) shows a huge enhancement, which for a large range of intensities is even better than the

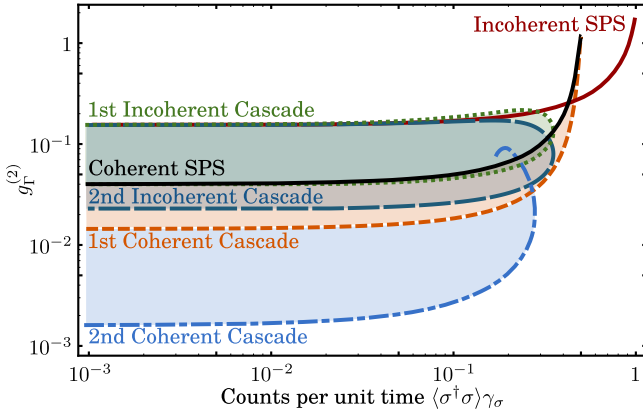


FIG. 11. Improvement in the $g_r^{(2)}$ due to the cascaded scheme. Once the linewidth of the first SPS is fixed, the degree of freedom of the second SPS spans a new accessible region shown by the color shading. The antibunching provided by an incoherent SPS is enhanced by the cascaded scheme, but for a wide range of parameters it is overcome by the antibunching provided by the coherent SPS. However, by allowing all the SPS in the cascade to be driven by a coherent field, a destructive interference sets limits on the enhancement of the $g_r^{(2)}$ at the first step. The enhancement on the second cascade is obtained by driving the cascade with only the emission of the coherent SPS. In the axis, γ_σ has the dimension of inverse time and its numerical value sets the unit.

antibunching for the second step in the incoherent cascade (large-dashed, blue line). However, the second step in the coherent cascade shows the same antibunching as the coherent SPS, thus effectively reducing its antibunching. In fact, if all the SPS in the cascade have the same decay rate, then all the even steps in the coherent cascade have the antibunching of the coherent SPS, whereas the odd steps have the antibunching of the first step in the coherent cascade. Another possible configuration for the coherent cascade provides a gain in the $g_r^{(2)}$ in the second step of the cascade, namely, removing the coherent excitation from all the SPS except for the first one. This is achieved in the same way as in Sec. II, for which Eq. (29) is modified to:

$$\begin{aligned} \partial_t \rho = & \sum_{j=1}^N \left(i[\rho, H_j] + \frac{\gamma_k}{2} \mathcal{L}_{c_k} \right) \rho - \sqrt{\epsilon \gamma_1} [\mathcal{E} c_1^\dagger - \mathcal{E}^* c_1, \rho] \\ & + \sum_{j=3}^N \sum_{l=2}^{j-1} \sqrt{\gamma_j \gamma_l} \{ [c_l \rho, c_j^\dagger] + [c_j, \rho c_l^\dagger] \} \\ & + \sum_{j=2}^N \sqrt{(1-\epsilon) \gamma_1 \gamma_j} \{ [c_1 \rho, c_j^\dagger] + [c_j, \rho c_1^\dagger] \}. \end{aligned} \quad (34)$$

The coherent SPS provided by Eq. (34) has the same antibunching as the one provided by Eq. (29), but requires a larger amplitude of the coherent field \mathcal{E} as it is effectively reduced by a factor $\sqrt{\epsilon}$. For a large range of values of the emission rate, the antibunching of the first step in the cascade coincides with the values obtained with Eq. (29). However, only a fraction $1 - \epsilon$ of the light emitted by the coherent SPS is transmitted to the cascade, so the emission rate of

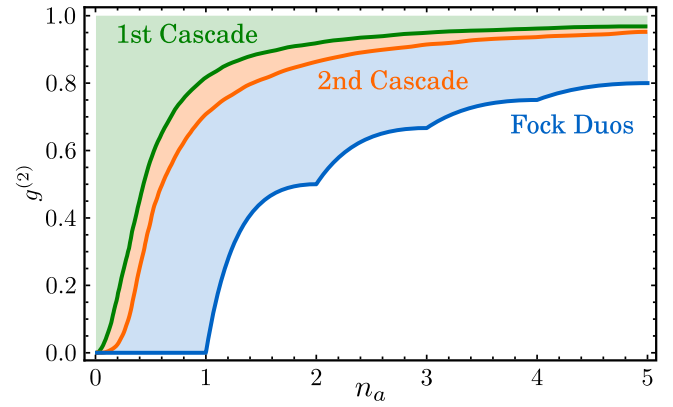


FIG. 12. Getting closer to the limit: adding a cascade step to excite a harmonic oscillator pushed the border of the accessible states from the green (first cascade) to the orange (second cascade) region. Adding more steps to the cascade could take the accessible region closer to the Fock Duos limit.

the cascade is reduced by that factor. This is shown by the dashed, golden line in Fig. 11. The antibunching for the second step in the cascade, as opposed to what is obtained with Eq. (29), improves vastly as shown by the dashed, blue line in Fig. 11. Considering, e.g., a typical lifetime of $\tau_\sigma = 1$ ns for a self-assembled quantum dot, whose transform limit turns into a photoluminescence (PL) line of $\gamma_\sigma = \hbar/\tau_\sigma = 666$ eV (power broadened by pumping), one gets emission rates of 10^7 counts per second with an antibunching of $\approx 3.5 \times 10^{-3}$ in a frequency window of $4\gamma_\sigma$ with two cascades under incoherent pumping, and one order of magnitude better antibunching with coherent pumping. The cascading can be iterated further and by turning to shorter-lived two-level emitters since we have removed the spectral constraint of outliers spoiling the antibunching, we can reach extremely bright antibunched single-photon sources. To appreciate these results, one can stress the saturated antibunching for the incoherent (red) and coherent (black) uncascaded SPS while SPSs in the cascades better their antibunching, albeit at the cost of diminished emission rates. This is because the first SPS sets the unit of time. In fact, the envelope of the first cascade, in the units fixed by the first SPS, is the same as the envelope of this first SPS. As a consequence, what one achieves already at the first case of the cascade is to increase the decay rate of the SPS for a given value of the antibunching, thereby achieving brighter single single-photon sources. Next stages in the cascade further improve the situation.

B. Comparison with the excitation of an harmonic oscillator

In Paper I [5], we treated the excitation of a harmonic oscillator by a quantum source. Such excitation allowed the harmonic oscillator to cover some area in the $(n_a, g^{(2)})$ space, shown in green in Fig. 12(a). Since this was some distance away from physical limit, a natural question is whether other quantum sources could access more territory. We now show how, indeed, the emission from a cascaded SPS achieves that goal, although still not yet touching the boundary. In the case of driving the oscillator with cascaded SPS, the excitation is obtained

by adding $(\gamma_a/2)\mathcal{L}_a\rho + \sqrt{\gamma_\sigma\gamma_a}\{[\sigma\rho, a^\dagger] + [a, \rho\sigma^\dagger]\} + \sqrt{\gamma_\xi\gamma_a}\{[\xi\rho, a^\dagger] + [a, \rho\xi^\dagger]\}$ to Eq. (1). Here, γ_a is the decay rate, and a the annihilation operator of the harmonic oscillator. In this configuration, the accessible area expands to the orange region of Fig. 12. Inspired by the positive results obtained using a second cascade to excite the harmonic oscillator, one might think that further cascading the source could move the border of the accessible states closer to the limit set by the Fock duo. However, covering all the possible values for all the free parameters (driving intensity, decay rates, and frequencies) grows exponentially with the number of cascades in the hypothetical device. It remains an open question at the time of writing as to whether further cascades, or for that matter another quantum source, can get closer or even reach the frontier.

VI. CONCLUSIONS

We have studied in detail several aspects as well as several configurations of the driving of a two-level system (2LS) by quantum light (and classical light for comparison). We have shown that the 2LS is “quantum enough” not to benefit by itself from the excitation by quantum light as far as the quantum state is concerned since classical excitation can drive it to the same steady state. However, when granted together with its source, with which it can enter in strong coupling, or when considering dynamical aspects of its emission, quantum driving of a SPS can result in new regimes for its dynamics. This led us to a discussion of the meaning and definition of strong coupling between states in absence of feedback and, therefore, of oscillations.

At a fundamental level, we have meticulously discussed all the main possibilities to drive a 2PS with various types of light, yielding a series of Mollow triplets that are summarized in Fig. 9. As the most elaborate description, we have presented a full quantized model where the lasing is self-consistently formed out of incoherent excitation through the one-atom lasing mechanism. This allows to consider aspects such as the question of the optical phase and the nature of the Rayleigh peak in absence of any c -number in the Hamiltonian.

At an applied level, we have shown how the quality of the reduction of multiple-photon emission (antibunching) is linked to the spectral tails. We identified in this way why coherent pumping (resonance fluorescence) overtakes its incoherent counterpart and discussed the counterintuitive Heitler effect of antibunched scattered photons off a laser. Namely, the coherent driving leads, in the weak coupling of the Mollow triplet, to interferences that turn the luminescence line into a Student- t distribution with weaker fat tails than the Lorentzian profile of spontaneous emission. This allows to collect more easily all the signal that, when taken in its entirety, results in a single emitted photon by destructive interferences of the possible emissions. We have shown how a similar and even further trimming of fat tails can be achieved by cascading SPS with the effect of yielding increasingly antibunched emitters with decreasing tails, ultimately converging towards a normal distribution (with no outliers), making it contemplable to thus design *perfect* single-photon sources, i.e., that yield exactly zero coincidence and perfect antibunching, $g^{(2)} = 0$, by considering, say, the emission in five standard deviations of

the cascaded SPS with enough stages to approach a Gaussian. This would provide one spurious coincidence in 3.5×10^6 repetitions, making any departure from exactly zero to any other factor in the experiment than the source itself. These results should stimulate experiments on new approaches to design better single-photon sources.

ACKNOWLEDGMENT

Funding by the POLAFLOW ERC Project No. 308136 and by the Spanish MINECO under Contract No. FIS2015-64951-R (CLAQUE) is acknowledged.

APPENDIX A: MASTER EQUATION FOR THE CASCADE OF TWO SYSTEMS

The theory of cascaded systems [54] allows to couple unidirectionally two quantum systems, so that one of them can be regarded as the source of the excitation that the other one receives, thus behaving as an optical target. The formalism is based on writing the Langevin equation for the operators of the two systems:

$$\begin{aligned} \dot{a}_1 = & i[a_1, H_{\text{sys}}] - [a_1, c_1^\dagger] \left\{ \frac{\gamma_1}{2} c_1 + \sqrt{\gamma_1} b_{\text{in}}^{(1)} \right\} \\ & + \left\{ \frac{\gamma_1}{2} c_1^\dagger + \gamma_1 b_{\text{in}}^{\dagger(1)} \right\} [a_1, c_1], \end{aligned} \quad (\text{A1a})$$

$$\begin{aligned} \dot{a}_2 = & i[a_2, H_{\text{sys}}] - [a_2, c_2^\dagger] \left\{ \frac{\gamma_2}{2} c_2 + \sqrt{\gamma_2} b_{\text{in}}^{(2)} \right\} \\ & + \left\{ \frac{\gamma_2}{2} c_2^\dagger + \gamma_2 b_{\text{in}}^{\dagger(2)} \right\} [a_2, c_2], \end{aligned} \quad (\text{A1b})$$

where a_k is any operator of system k that decays at a rate γ_k , $H_{\text{sys}} = H_1 + H_2$ is the total Hamiltonian, describing the *independent* dynamics of the two systems, and $b_{\text{in}}^{(k)}$ is the input field of system k . Since we are considering that the system 2 (the target) is driven by the emission of system 1 (the source), it is clear that the input field of system 2 corresponds to the output field of system 1:

$$b_{\text{in}}^{(2)} = b_{\text{in}}^{(1)} + \sqrt{\gamma_1} c_1, \quad (\text{A2})$$

where the last term of the right-hand side describes the emission of system 1, due only to its internal dynamics. Converting Eq. (A1) to a quantum Ito equation and assuming that the input field has an amplitude \mathcal{E} , we can obtain a master equation for the operator $\rho(t)$ describing the cascaded system, which takes the form:

$$\begin{aligned} \partial_t \rho = & i[\rho, H_1 + H_2] + \frac{\gamma_1}{2} \mathcal{L}_{c_1} \rho + \frac{\gamma_2}{2} \mathcal{L}_{c_2} \rho \\ & - [\mathcal{E}(\sqrt{\gamma_1} c_1^\dagger + \sqrt{\gamma_2} c_2^\dagger) - \mathcal{E}^*(\sqrt{\gamma_1} c_1 + \sqrt{\gamma_2} c_2), \rho] \\ & + \sqrt{\gamma_1 \gamma_2} \{ [c_1 \rho, c_2^\dagger] + [c_2, \rho c_1^\dagger] \}, \end{aligned} \quad (\text{A3})$$

which is the equation to which we refer to in Sec. II. We note that the second line in Eq. (B3) is a Hamiltonian-type term, that describes the coherent driving of the two systems in the cascade.

APPENDIX B: MASTER EQUATION FOR THE CASCADE OF AN ARBITRARY NUMBER OF SYSTEMS

The formalism presented in Appendix A can be generalized to the cascade of an arbitrary number of systems. In such case, each operator of the k th system would satisfy the Langevin equation:

$$\dot{a}_k = i[a_k, H_{\text{sys}}] - [a_k, c_k^\dagger] \left\{ \frac{\gamma_k}{2} c_k \sqrt{\gamma_k} b_{\text{in}}^{(k)} \right\} \quad (\text{B1})$$

$$+ \left\{ \frac{\gamma_k}{2} c_k^\dagger + \gamma_k b_{\text{in}}^{\dagger(k)} \right\} [a_k, c_k], \quad (\text{B2})$$

where now the input field of the k th system corresponds to the output field of the $(k-1)$ th system, i.e., $b_{\text{in}}^{(k)} = b_{\text{in}}^{(1)} + \sum_{j=1}^{k-1} \sqrt{\gamma_j} c_j$. As in Appendix A, we can derive the master equation for operator $\rho(t)$ describing the cascaded system:

$$\begin{aligned} \partial_t \rho = & \sum_{j=1}^N \left(i[\rho, H_j] + \frac{\gamma_k}{2} \mathcal{L}_{c_k} \rho - \sqrt{\gamma_j} [\mathcal{E} c_j^\dagger - \mathcal{E}^* c_j, \rho] \right) \\ & + \sum_{j=2}^N \sum_{l=1}^{j-1} \sqrt{\gamma_j \gamma_l} \{ [c_l \rho, c_j^\dagger] + [c_j, \rho c_l^\dagger] \}, \end{aligned} \quad (\text{B3})$$

which is the equation that we refer to in Sec. V.

-
- [1] R. P. Feynman, R. B. Leighton, and M. Sands, *The Feynman Lectures on Physics*, Vol. III (Addison Wesley, Boston, 1971).
- [2] D. Deutsch, Quantum theory, the Church-Turing principle and the universal quantum computer, *Proc. R. Soc. London, Ser. A* **400**, 97 (1985).
- [3] N. V. Golubev and A. I. Kuleff, Control of populations of two-level systems by a single resonant laser pulse, *Phys. Rev. A* **90**, 035401 (2014).
- [4] L. Allen, and J. H. Eberly, *Optical Resonance and Two-Level Atoms* (Dover, New York, 1987).
- [5] J. C. López Carreño and F. P. Laussy, Excitation with quantum light. I. Exciting a harmonic oscillator, *Phys. Rev. A* **94**, 063825 (2016).
- [6] B. R. Mollow, Power spectrum of light scattered by two-level systems, *Phys. Rev.* **188**, 1969 (1969).
- [7] I. Bengtsson and K. Życzkowski, *Geometry of Quantum States* (Cambridge University Press, Cambridge, 2008).
- [8] R. P. Feynman, F. L. Vernon, Jr., and R. W. Hellwarth, Geometrical representation of the Schrödinger equation for solving Maser problems, *J. Appl. Phys.* **28**, 49 (1957).
- [9] E. Jaynes and F. Cummings, Comparison of quantum and semiclassical radiation theory with application to the beam maser, *Proc. IEEE* **51**, 89 (1963).
- [10] E. del Valle, F. P. Laussy, and C. Tejedor, Luminescence spectra of quantum dots in microcavities. II. Fermions, *Phys. Rev. B* **79**, 235326 (2009).
- [11] N. Quesada, Strong coupling of two quantum emitters to a single light mode: The dissipative Tavis-Cummings ladder, *Phys. Rev. A* **86**, 013836 (2012).
- [12] E. del Valle and F. P. Laussy, Regimes of strong light-matter coupling under incoherent excitation, *Phys. Rev. A* **84**, 043816 (2011).
- [13] C. N. Cohen-Tannoudji and S. Reynaud, Dressed-atom description of resonance fluorescence and absorption spectra of a multi-level atom in an intense laser beam, *J. Phys. B: At. Mol. Phys.* **10**, 345 (1977).
- [14] E. del Valle and F. P. Laussy, Mollow Triplet Under Incoherent Pumping, *Phys. Rev. Lett.* **105**, 233601 (2010).
- [15] F. P. Laussy, E. del Valle, and C. Tejedor, Luminescence spectra of quantum dots in microcavities. I. Bosons, *Phys. Rev. B* **79**, 235325 (2009).
- [16] W. Weisskopf, and E. Wigner, Calculation of the natural line width on the basis of Dirac's theory of light (as translated by J. B. Sykes), *Z. Phys.* **63**, 54 (1930).
- [17] W. Heitler, *The Quantum Theory of Radiation* (Oxford University Press, Oxford, 1944).
- [18] H. S. Nguyen *et al.*, Ultra-coherent single photon source, *Appl. Phys. Lett.* **99**, 261904 (2011).
- [19] C. Matthiesen, A. N. Vamivakas, and M. Atatüre, Subnatural Linewidth Single Photons from a Quantum Dot, *Phys. Rev. Lett.* **108**, 093602 (2012).
- [20] R. Proux, M. Maragkou, E. Baudin, C. Voisin, P. Roussignol, and C. Diederichs, Measuring the Photon Coalescence Time Window in the Continuous-Wave Regime for Resonantly Driven Semiconductor Quantum Dots, *Phys. Rev. Lett.* **114**, 067401 (2015).
- [21] R. Al-Khuzheyri *et al.*, Resonance fluorescence from a telecom-wavelength quantum dot, [arXiv:1607.02063](https://arxiv.org/abs/1607.02063).
- [22] A. González-Tudela, F. P. Laussy, C. Tejedor, M. J. Hartmann, and E. del Valle, Two-photon spectra of quantum emitters, *New J. Phys.* **15**, 033036 (2013).
- [23] F. P. Laussy, E. del Valle, and J. Finley, Universal signatures of lasing in the strong coupling regime, *Proc. SPIE* **8255**, 82551G (2012).
- [24] P. Zoller, Emission spectra of atoms strongly driven by finite bandwidth laser light, *J. Phys. B: At. Mol. Phys.* **11**, 805 (1978).
- [25] P. Zoller, Atomic relaxation and resonance fluorescence in intensity and phase-fluctuating laser light, *J. Phys. B: At. Mol. Phys.* **11**, 2825 (1978).
- [26] P. Zoller and F. Ehlötzky, Resonance fluorescence in phase-frequency modulated laser fields, *Z. Phys. A* **285**, 245 (1978).
- [27] Y. Mu and C. M. Savage, One-atom lasers, *Phys. Rev. A* **46**, 5944 (1992).
- [28] J. McKeever, A. Boca, A. D. Boozer, J. R. Buck, and H. J. Kimble, Experimental realization of a one-atom laser in the regime of strong coupling, *Nature (London)* **425**, 268 (2003).
- [29] M. Nomura, N. Kumagai, S. Iwamoto, Y. Ota, and Y. Arakawa, Laser oscillation in a strongly coupled single-quantum-dot-nanocavity system, *Nat. Phys.* **6**, 279 (2010).
- [30] F. Gericke *et al.*, Coexistence of lasing and strong coupling in quantum-dot microlasers, [arXiv:1606.05591](https://arxiv.org/abs/1606.05591).
- [31] L. A. Whitehead, Domino "chain reaction", *Am. J. Phys.* **51**, 182 (1983).
- [32] R. L. Lindeman, The trophic-dynamic aspect of ecology, *Ecology* **23**, 399 (1942).
- [33] M. Bodenstern, Eine theorie der photochemischen reaktionsgeschwindigkeiten, *Z. Phys. Chem.* **85**, 390 (1913).

- [34] H. L. Anderson, E. Fermi, and L. Szilard, Neutron production and absorption in uranium, *Phys. Rev.* **56**, 284 (1939).
- [35] R. H. Dicke, Coherence in spontaneous radiation processes, *Phys. Rev.* **93**, 99 (1954).
- [36] A. L. Schawlow and C. H. Townes, Infrared and optical masers, *Phys. Rev.* **112**, 1940 (1958).
- [37] R. F. Kazarinov and R. Suris, Possibility of amplification of electromagnetic waves in a semiconductor with a superlattice, *Fiz. Tekh. Poluprovodn.* **5**, 797 (1971) [*Sov. Phys. Semicond.* **5**, 707 (1971)].
- [38] J. Faist *et al.*, Quantum cascade laser, *Science* **264**, 553 (1994).
- [39] T. C. H. Liew, M. M. Glazov, K. V. Kavokin, I. A. Shelykh, M. A. Kaliteevski, and A. V. Kavokin, Proposal for a Bosonic Cascade Laser, *Phys. Rev. Lett.* **110**, 047402 (2013).
- [40] T. C. H. Liew *et al.*, Quantum statistics of bosonic cascades, *New J. Phys.* **18**, 023041 (2016).
- [41] H. Paul, Photon antibunching, *Rev. Mod. Phys.* **54**, 1061 (1982).
- [42] S. Aaronson and A. Arkhipov, The computational complexity of linear optics, in *Proceedings of the 43rd Annual ACM Symposium on Theory of Computing* (ACM, New York, 2011), p. 333.
- [43] M. Rau *et al.*, Free space quantum key distribution over 500 meters using electrically driven quantum dot single-photon sources: A proof of principle experiment, *New J. Phys.* **16**, 043003 (2014).
- [44] A. Schlehahn *et al.*, Single-photon emission at a rate of 143 MHz from a deterministic quantum-dot microlens triggered by a mode-locked vertical-external-cavity surface-emitting laser, *Appl. Phys. Lett.* **107**, 041105 (2015).
- [45] X. Ding, Y. He, Z. C. Duan, N. Gregersen, M. C. Chen, S. Unsleber, S. Maier, C. Schneider, M. Kamp, S. Hofling, C. Y. Lu, and J. W. Pan, On-Demand Single Photons with High Extraction Efficiency and Near-Unity Indistinguishability from a Resonantly Driven Quantum Dot in a Micropillar, *Phys. Rev. Lett.* **116**, 020401 (2016).
- [46] A. V. Kuhlmann *et al.*, Transform-limited single photons from a single quantum dot, *Nat. Commun.* **6**, 8204 (2015).
- [47] S. Unsleber *et al.*, Highly indistinguishable on-demand resonance fluorescence photons from a deterministic quantum dot micropillar device with 74% extraction efficiency, *Opt. Express* **24**, 8539 (2016).
- [48] N. Somaschi *et al.*, Near-optimal single-photon sources in the solid state, *Nat. Photonics* **10**, 340 (2016).
- [49] J. C. Loredó *et al.*, Scalable performance in solid-state single-photon sources, *Optica* **3**, 433 (2016).
- [50] J. Petersen, J. Volz, and A. Rauschenbeutel, Chiral nanophotonic waveguide interface based on spin-orbit interaction of light, *Science* **346**, 67 (2014).
- [51] R. J. Coles *et al.*, Chirality of nanophotonic waveguide with embedded quantum emitter for unidirectional spin transfer, *Nat. Commun.* **7**, 11183 (2016).
- [52] Y. Ma, G. Ballesteros, J. M. Zajac, J. Sun, and D. B. Gerardot, Highly directional emission from a quantum emitter embedded in a hemispherical cavity, *Opt. Lett.* **40**, 2373 (2015).
- [53] H. M. Meyer, R. Stockill, M. Steiner, C. LeGall, C. Matthiesen, E. Clarke, A. Ludwig, J. Reichel, M. Atatüre, and M. Kohl, Direct Photonic Coupling of a Semiconductor Quantum Dot and a Trapped Ion, *Phys. Rev. Lett.* **114**, 123001 (2015).
- [54] G. W. Gardiner and P. Zoller, *Quantum Noise*, 2nd ed. (Springer, Berlin, 2000).
- [55] E. del Valle, A. González-Tudela, F. P. Laussy, C. Tejedor, and M. J. Hartmann, Theory of Frequency-Filtered and Time-Resolved n -Photon Correlations, *Phys. Rev. Lett.* **109**, 183601 (2012).